NREL/SR--520-24854

June 1998 • NREL/SR-520-24854

Amorphous Silicon Research

Final Technical Report
13 September 1994 – 28 February 1998

R. Arya, D. Carlson, L. Chen, G. Ganguly, M. He, G. Lin, R. Middya, S. Skibo, and G. Wood
Solarex, a Business Unit of Amoco/Enron Solar
Newtown, Pennsylvania

National Renewable Energy Laboratory
1617 Cole Boulevard
Golden, Colorado 80401-3393
A national laboratory of
the U.S. Department of Energy
Managed by Midwest Research Institute
for the U.S. Department of Energy
under Contract No. DE-AC36-83CH10093

NREL/SR-520-24854

Amorphous Silicon Research

Final Technical Report
13 September 1994 – 28 February 1998

R. Arya, D. Carlson, L. Chen, G. Ganguly, M. He, G. Lin, R. Middya, S. Skibo, and G. Wood
Solarex, a Business Unit of Amoco/Enron Solar
Newtown, Pennsylvania

NREL technical monitor: K. Zweibel

National Renewable Energy Laboratory
1617 Cole Boulevard
Golden, Colorado 80401-3393
A national laboratory of
the U.S. Department of Energy
Managed by Midwest Research Institute
for the U.S. Department of Energy
under Contract No. DE-AC36-83CH10093

Prepared under Subcontract No. ZAN-4-13318-01
June 1998

This publication was reproduced from the best available camera-ready copy submitted by the subcontractor and received no editorial review at NREL.

NOTICE

Available to DOE and DOE contractors from:
Office of Scientific and Technical Information (OSTI)
P.O. Box 62
Oak Ridge, TN 37831
Prices available by calling (423) 576-8401

Available to the public from:
National Technical Information Service (NTIS)
U.S. Department of Commerce
5285 Port Royal Road
Springfield, VA 22161
(703) 487-4650

Printed on paper containing at least 50% wastepaper, including 20% postconsumer waste

DISCLAIMER

1. Executive Summary

This report describes the Solarex R&D effort as part of the Thin Film Partnership with NREL under Subcontract No. ZAN - 4 - 13318 – 01. The major goal of this program has been to develop the device and processing technology necessary to commercialize large-area amorphous silicon tandem PV modules. There were three major areas of investigation in this program: (1) research on mid-gap amorphous silicon alloys; (2) research on low-bandgap amorphous silicon alloys; and (3) research on multijunction devices and modules.

The effort on mid-gap alloys has been largely focused on understanding and reducing the light-induced degradation that occurs in all amorphous silicon alloys. This investigation showed that many of the metastable centers are charged both under illumination and in the dark and that the annealing recovery of the degradation could be accelerated significantly by the application of a strong reverse bias. The experimental observations have been modeled assuming that the accelerated recovery is associated with the local motion of protons near dangling bonds. According to this model, the metastable defects can be created when an electron is trapped at a weak Si-Si bond and a hole localizes on a nearby Si-H bond; the hydrogen atom can then move as a proton to the negatively charged weak bond creating a new Si-H bond and two separated dangling bonds.

Amorphous silicon germanium alloys have been grown using both hydrogen and helium dilution, and the stabilized performance of both single-junction and tandem cells grown using either diluent are comparable. However, the deposition rates are typically about 20% higher for amorphous silicon germanium films grown with helium dilution as compared to control devices made with hydrogen dilution.

The performance of amorphous silicon solar cells can be strongly influenced by residual contaminants on the tin oxide coated glass. In particular, commercial tin oxide coated glass is usually coated with protective layers that are difficult to remove with standard cleaning techniques. Good contacts to the tin oxide can be obtained if the substrates are cleaned in an ultrasonic detergent bath.

Part of the research effort has been directed at increasing throughput and reducing materials costs. This work has involved the development of a fast recombination junction process for the tandem structure, the investigation of helium dilution as a means of increasing the deposition rate and the development of a two step process that decreases the deposition time for the intrinsic layers. This effort has resulted in a reduction of 21% in processing time for the deposition of the tandem structure and an increase of 30% in the utilization of feedstock gases.

The tandem process was scaled up to 4 ft^2 in a pilot production mode, and initial conversion efficiencies averaged about 9.5% for runs of 40 modules. Based on light soaking data on similar modules, the stabilized conversion efficiency was projected to be about 8.1% for these modules. In 1997, the tandem process was transferred to a Solarex plant in Virginia that has the capacity to produce 10 MW of 8.6 ft^2 tandem modules per year.

2. Table of Contents

2.1 List of Figures

List of Tables

3. Introduction

The major objectives of this research program have been to: (i) demonstrate a stabilized conversion efficiency of 8% in large-area tandem modules, and (ii) scale up the multijunction technology from 1 to 8.6 ft^2 and transfer the technology to the Solarex plant in Virginia. The technical program consisted of three major tasks: Task 1, mid-bandgap alloy research; Task 2, low-bandgap alloy research; and Task 3, multijunction devices and modules.

4. Technical Program

4.1 Task 1: Mid-bandgap Alloy Research

4.1.1 Field-Enhanced Recovery of Light-Induced Degradation

The light-induced degradation of the optoelectronic properties of hydrogenated amorphous silicon (a-Si:H) was discovered in 1977 by Staebler and Wronski [1]. They showed that the degradation was reversible and that the initial properties could be recovered by annealing the a-Si:H films at temperatures of ~ 200^0C in the dark. Shortly thereafter, it was shown that prolonged light exposure would also degrade the performance of amorphous silicon solar cells and that the degradation of the cells could be suppressed by applying a strong reverse bias to the cells while illuminated [2]. More recent work has shown that the light-induced degradation can be at least partially removed by applying a reverse bias during illumination [3].

Other studies have shown that the metastable defects are associated with silicon dangling bonds [4] that are created by the recombination or trapping of photogenerated or injected carriers, and that both charged and neutral dangling bonds are created [5]. The Staebler-Wronski effect is observed in all device-quality amorphous silicon alloys, and despite almost two decades of intense research efforts, a-Si:H solar cells still exhibit light-induced degradation on the order of ~ 10 to 30% depending on the deposition conditions and the device structure.

Recently we have shown that the light-induced degradation in a-Si:H solar cells can be totally reversed by the application of a strong reverse bias while the cells are exposed to intense illumination at normal operating temperatures. The rate of reversal was found to depend strongly on the strength of the electric field, the temperature and the light intensity.

The a-Si:H solar cells used in the present study were single-junction p-i-n cells (0.27 cm^2) that were fabricated using tin oxide coated glass substrates and rear contacts of zinc oxide/aluminum[6]; the i-layers were ~ 260 to 350 nm thick. The initial conversion efficiencies of the cells were typically about 9% with open-circuit voltages of ~ 0.91 V, short-circuit current densities of ~ 14 mA/cm^2 and fill factors of ~ 0.7. A xenon arc lamp was used to illuminate the cells with high intensity white light (up to 60 suns), and the temperature was controlled by adjusting the flow of nitrogen gas that was directed onto the cell. The temperature of each treated cell was measured using a thin foil (0.0005") thermocouple that was cemented to the back contact of the cell with a high thermal conductivity, electrically insulating paste.

In one series of experiments, a number of identical p-i-n cells were exposed to 60 suns illumination at 65^{0}C for 20 minutes while under open-circuit conditions. As shown in Fig. 1, this exposure caused the conversion efficiency of the cells to fall by ~ 33%. (Exposing these cells to 1 sun illumination for 600 hours caused the efficiency to fall by ~ 23%.) These cells were then exposed to 60 suns illumination for an additional 70 minutes at various temperatures and bias conditions. If the cell was maintained in the open-circuit mode at 65^{0}C, then the efficiency fell by about another 5% during the additional 70 minute exposure.

However, if the cell was subjected to a reverse bias of - 6 V at 65^{0}C, then the conversion efficiency actually started to improve with continued exposure to the 60 suns illumination. As shown in Fig. 1, the normalized conversion efficiency fell to about 0.67 after the first 20 minutes in the open circuit mode, but then increased to about 0.80 after an additional 70 minutes exposure to 60 suns at - 6 V reverse bias. Repeating the experiment with the same initial 20 minute exposure at 65^{0}C, but then increasing the temperature to 125^{0}C before continuing the 60 suns exposure at - 6 V caused the cell to recover its performance in about 30 minutes.

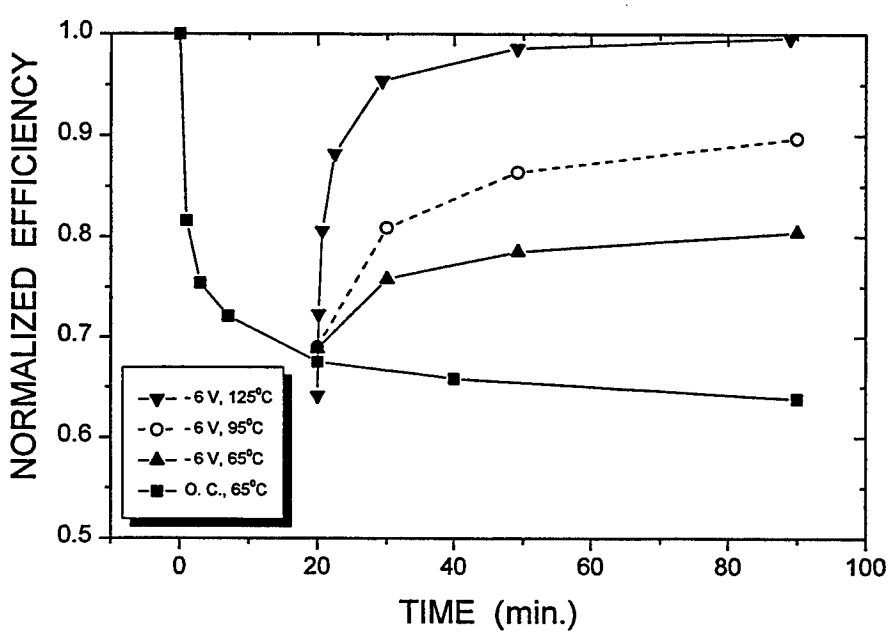

Fig. 4.1 The normalized conversion efficiency as a function of time for a series of a-Si:H p-i-n solar cells that were exposed to 60 suns illumination under open circuit conditions and then to a reverse bias of –6V at various temperatures.

One can define a characteristic recovery time as the time it takes for a cell to recover 50% of the loss in performance. Applying this definition to the data in Fig. 4.1 and plotting the data in an Arrhenius plot gives an activation energy on the order of 0.9 eV.

While the recovery rate of the light-induced degradation is strongly dependent on temperature, the degradation rate is only weakly temperature dependent over the range of 39^{0}C to 90^{0}C. This behavior is expected since the metastable defect creation rate is only

weakly temperature dependent [7]. In the first two minutes of exposure to 60 suns under open circuit conditions, all cells degraded about 20% independent of temperature. However, after 20 minutes of exposure, cells maintained at 39^{0}C degraded about 37% while those at 90^{0}C exhibited only about 30% degradation due to increased annealing effects.

In another series of experiments, several cells were exposed to 50 suns illumination at 60^{0}C for 30 minutes while under open-circuit conditions and were then subjected to various reverse biases while exposed to 50 suns at 100^{0}C. As shown in Fig. 4.2, the magnitude of the reverse bias had a strong effect on the recovery rate. After exposure to 50 suns at 100^{0}C under short-circuit conditions, the cells recovered ~ 36% of their performance loss in 20 minutes. After a similar exposure at a reverse bias of - 6 V, the percentage of performance recovery increased to ~ 74%.

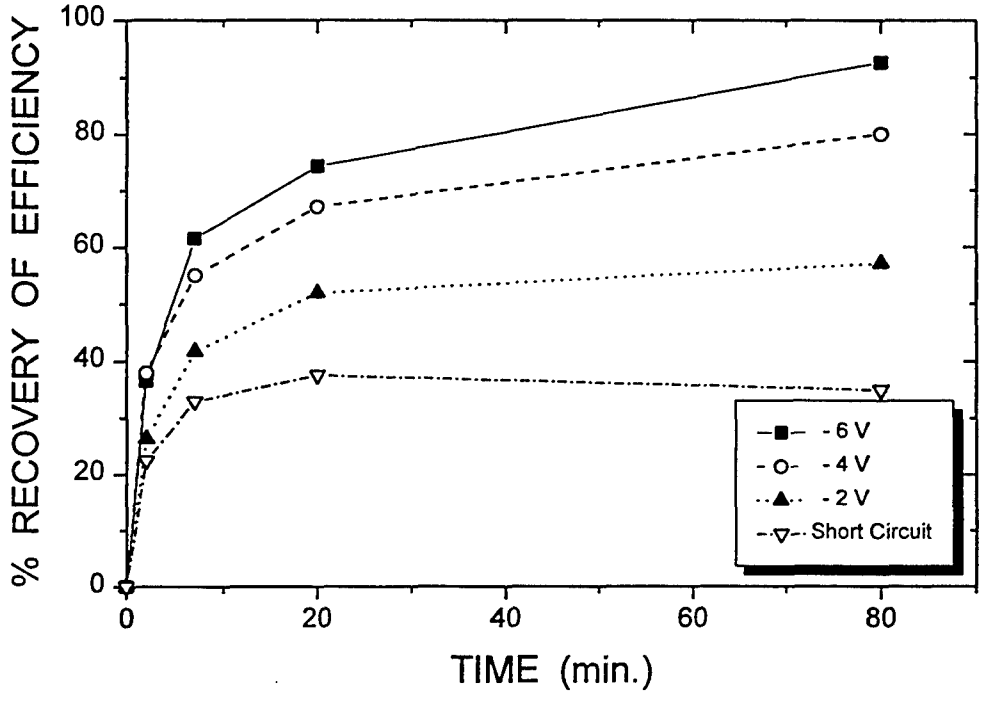

Fig. 4.2 The percentage of recovery of the conversion efficiency as a function of treatment time for degraded p-i-n cells subjected to different reverse biases while exposed to 50 suns at 100^{0}C.

The rate of recovery from light-induced degradation depends on both the reverse bias and the light intensity. Applying a reverse bias of - 6 V to a degraded p-i-n cell at 60^{0}C in the dark increased the recovery rate as compared to that due to annealing in the dark under open-circuit conditions (see Fig. 4.3). When an identical degraded cell was exposed to 10 suns at - 6 V, the recovery rate of the fill factor increased significantly over that in the dark. Increasing the light intensity to 50 suns increased the rate of recovery even further so that the fill factor recovered about 47% of its light-induced loss in 80 minutes at 60^{0}C.

When the p-i-n cells were exposed to several cycles of light-induced degradation and field-induced recovery, a small permanent loss in performance was observed. In another experiment, a few annealed p-i-n cells were exposed to 60 suns while under a continuous reverse bias of - 6 V at 95^{0}C. In this case, the performance improved slightly in the first few hours of exposure, and then gradually decreased as both the fill factor and short-circuit current density fell. After 15 hours of exposure, the conversion efficiency had fallen by a few %. After annealing the cells for 1 hour at 170^{0}C, the performance almost returned to its original value except for a small loss in the short-wavelength spectral response. An extrapolation of the degradation data observed at higher temperatures [8,9] indicates that this small irreversible degradation is probably due to field-driven proton motion near the p/i interface.

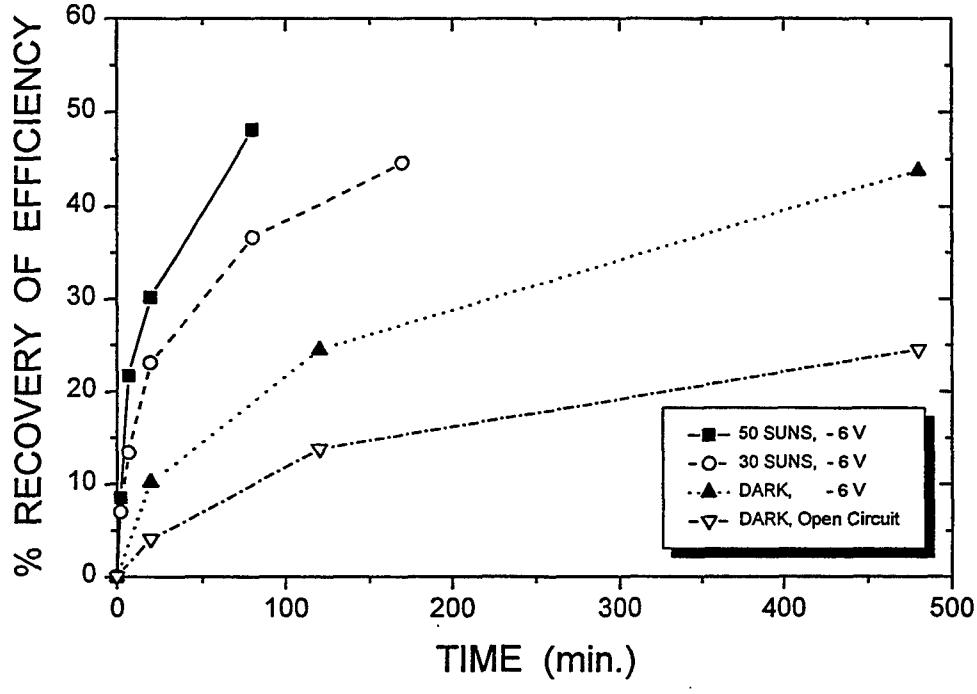

Fig. 4.3 The percentage of recovery of the conversion efficiency as a function of treatment time for degraded p-i-n cells under different bias and illumination conditions at 60^{0}C.

In an attempt to elucidate the roles of photogenerated electrons and holes in the recovery process, some cells were made in a n-i-p configuration (i.e. glass / zinc oxide / n-i-p / zinc oxide). These cells were degraded by exposure to 60 suns illumination through the glass substrate for 30 minutes at 60^{0}C while at open circuit, and then some cells were exposed to intense blue light incident through the n-layer while subjected to a reverse bias of - 5 V. The blue light was obtained with filters that transmitted mainly in the 420 - 460 nm wavelength range. The reverse bias photocurrent during illumination with the blue light was ~ 2.2 times larger than the short-circuit current density under 1 sun illumination.

The rate of recovery of the fill factor of these cells is shown as a function of exposure time in Fig. 4.4, and in all cases, the rate of recovery was enhanced as compared to that in the dark. The conversion efficiencies in this case were measured by illuminating through the p-layer, but the trends were similar when the efficiencies were measured by illuminating through the

n-layer. When the blue light is incident through the n-layer, most of the photogenerated carriers are created near the n-layer (the absorption coefficient is on the order of 2×10^5 cm^{-1}), and the holes are pulled across the device to the p-layer region by the strong internal field.

Similar results were obtained when degraded p-i-n cells where exposed to intense blue light through the p-layer while subjected to a reverse bias of - 6 V. When the blue light is incident through the p-layer, electrons are pulled across the device to the n-layer by the field. Thus, both photogenerated electrons and holes appear to be capable of increasing the rate of reversal of the light-induced degradation in the presence of a strong electric field. It is interesting to note that a reverse bias increased the recovery rate in the dark for p-i-n cells (see Figure 4.3), but the effect was not evident in the n-i-p cells (see Figure 4.4) indicating that the defects or charge states are different in these n-i-p cells.

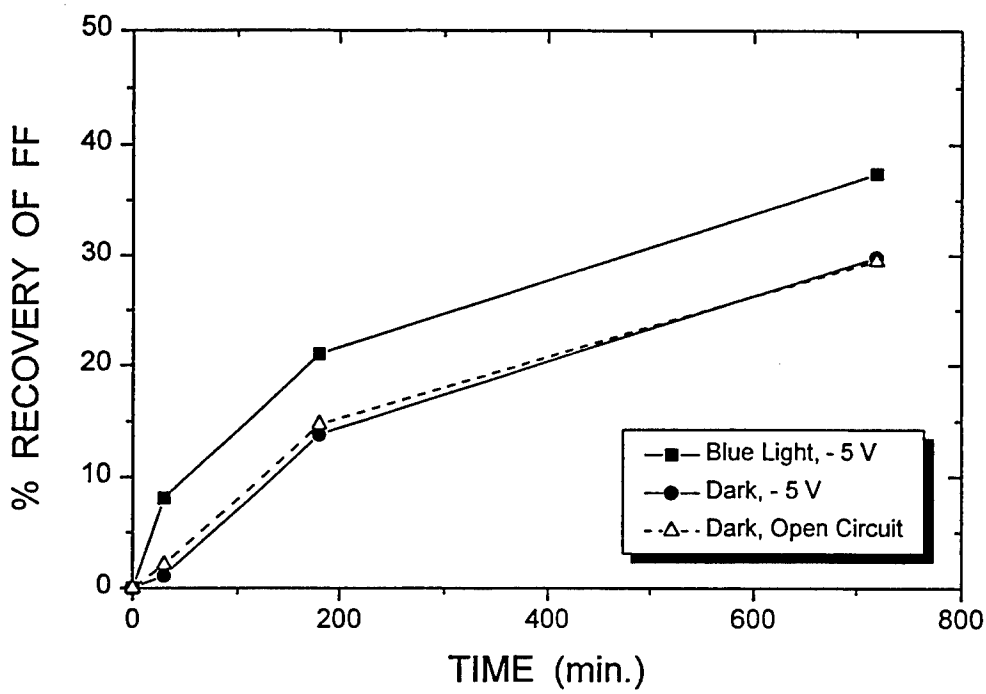

Fig. 4.4 The percentage of recovery of the fill factor as a function of treatment time for degraded n-i-p cells subjected to different bias and illumination conditions at 60^0C

The fact that a strong electric field can reverse the light-induced degradation indicates that many of the metastable centers in p-i-n cells must be charged even in the dark and that more of these centers may become charged when exposed to intense illumination. The strong field could be causing thermally-assisted field emission of either electrons or holes from the metastable defects or it could be inducing hydrogen ion motion. While field-driven proton motion appears to be causing some permanent degradation in the vicinity of the p/i interface for long exposures, it is possible that the field-induced recovery might be associated with short-range proton motion, possibly on the internal surfaces of microvoids [10].

It does not seem practical to use a strong reverse bias in the presence of intense illumination to reverse the degradation since the energy requirements are large. For the case of a 30 minute exposure to 60 suns at - 6 V at 125^0C (see Fig. 1), the energy required to reverse the

degradation is about 6 X 10^3 J/cm^2. The energy in the 60 suns light exposure is even greater, 1.08 X 10^4 J/cm^2. If one uses a light source that converts electricity into light at an efficiency of about 1%, then the energy requirement increases by a factor of 100. Under these circumstances, it would take about sixteen years of exposure to sunlight for a 10% efficient cell to generate the same amount of energy.

In more recent studies, we have observed that the annealing rate of the light-induced degradation of p-i-n cells in the dark at temperatures in the range of 60 to 100^{0}C is increased significantly by a strong reverse bias. The p-i-n cells in these studies were degraded by exposing them to 50 suns illumination from a focused Xe arc lamp for 30 minutes at 60^{0}C while at open-circuit. Under these conditions, the efficiencies would typically fall from about 8.3% to 6.5%, and the fill factors would fall from about 0.66 to 0.56.

In one series of experiments, we heated a degraded cell to 60^{0}C and then monitored the change in performance with time while the cell was exposed to different reverse biases in the dark. After monitoring the recovery of the cell performance for about 3000 minutes at a specific reverse bias, we then annealed the cell for 20 minutes at 170^{0}C to return the cell to an annealed state. The cell was then degraded again using the same degradation procedure mentioned above, and the recovery at 60^{0}C was then monitored at a different reverse bias voltage. As shown in Fig. 4.5, the application of a strong reverse bias at 60^{0}C in the dark caused a significant increase in the rate of recovery of the fill factor.

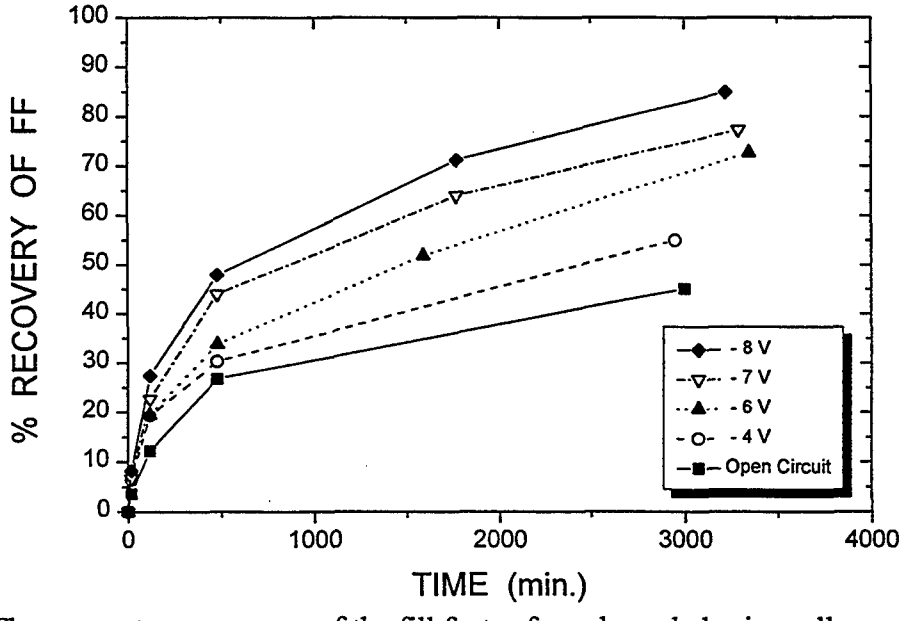

Fig. 4.5 The percentage recovery of the fill factor for a degraded p-i-n cell annealed at 60^{0}C in the dark under various bias conditions.

Similar series of experiments were performed on the same cell and on other cells at annealing temperatures ranging from 60 to 100^{0}C. In Fig. 4.6, we show data for the recovery of the fill factor for the same cell as represented in Fig. 4.5 where now the annealing temperature in the dark was 100^{0}C. While the recovery rates are much more rapid due to the elevated temperature, the same acceleration of the recovery by the applied field is clearly evident.

Earlier work [11] showed that the recovery rates were even more rapid when the cells were subjected to strong reverse biases under intense illumination.

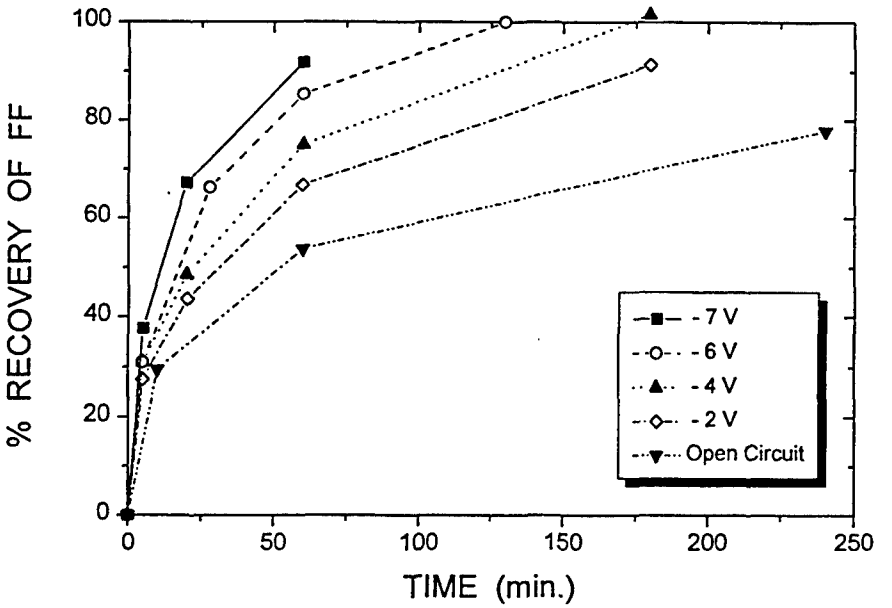

Fig. 4.6 The percentage recovery of the fill factor for a degraded p-i-n cell annealed at 100^0C in the dark under various bias conditions.

The data can be analyzed using a simple empirical model. Faughnan and Crandall [12] showed that the fill factor varied linearly with the collection length over a relatively wide range for a-Si:H p-i-n cells that were ~ 0.5 μm thick. Thus, if the electric field across the i-layer is relatively uniform, then FF $\propto \mu\tau E$ where μ and τ are averages of the mobilities and lifetimes for photogenerated electrons and holes, and E is the electric field across the i-layer during the measurement. The average lifetime should be inversely proportional to the density of metastable defects in the i-layer.

Since we start with the same degraded state in each case, the time for the fill factor to recover 50% of its total loss will be a measure of the time to remove a certain number of metastable defects. In Fig. 4.7, we show a plot of this characteristic recovery time as a function of the inverse temperature for cells annealed in the dark under open-circuit conditions and under a reverse bias of - 7 V. Also shown are data for cells that were exposed to 50 suns while under a reverse bias of - 6 V.

The activation energy of 1.34 eV for annealing in the dark under open-circuit conditions is close to that observed for hydrogen diffusion [13]. The application of a strong reverse bias lowers the activation energy somewhat while the additional application of intense illumination lowers the activation energy by ~ 0.57 eV as compared to that for open-circuit annealing in the dark. A similar large reduction in activation energy has been observed for hydrogen diffusion when a-Si:H is exposed to intense illumination [14]. The activation energies in the present case are somewhat lower than those observed for hydrogen diffusion in undoped a-

Si:H both in the dark and under intense illumination, but the barriers may be somewhat lower if the hydrogen motion is localized within a metastable defect complex.

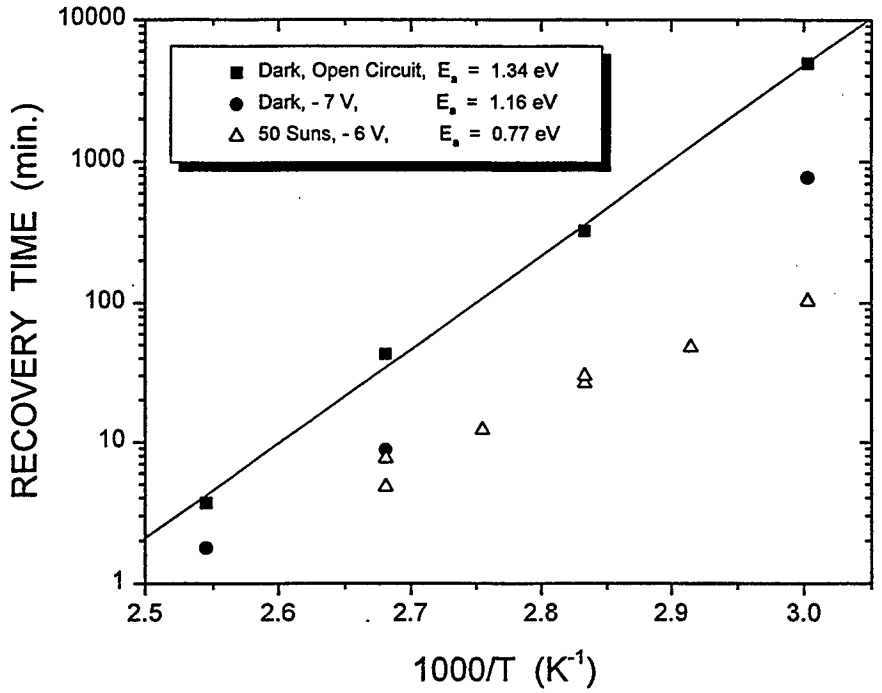

Fig. 4.7 Arrhenius plots of the recovery time for degraded p-i-n cells that were annealed under various illumination and bias conditions.

It is clear from the present study that the metastable defects in a-Si:H solar cells must readily trap charge and that a strong field can then induce the charged defect to revert back to the ground state. We hypothesize that both electronic and protonic events are involved in the creation and field-induced reversal of the metastable defects. As suggested by Dersch et al. [15], the metastable complex may consist of a Si-H bond near a weak Si-Si bond since these complexes are very likely to occur near the internal surfaces of microvoids as well as in bulk a-Si:H material. The weak Si-Si bond is very likely to trap photogenerated carriers while it is also possible for holes to be temporarily localized in the vicinity of the Si-H bond. Considering the case where an electron is trapped on the weak Si-Si bond and a hole is trapped near the Si-H bond, then one of three events could occur: (1) the electron could hop to the trapped hole and recombine, (2) the hole could hop to the trapped electron and recombine, or (3) the trapped hole weakens the Si-H bond and the charge localizes on the hydrogen allowing it to move as a proton to the trapped electron.

The first two events are much more likely to occur since the energy barriers associated with the electron and hole traps are relatively shallow and the attempt frequencies for escape are relatively high compared to the situation for proton motion. However, proton motion could still occur some small fraction of the time since the Si-H bond will be significantly weakened if the hole is localized there. (This is evident since the bonding energy of the H_2 molecule decreases by about 1.8 eV when it is ionized [16].) When the distance between the proton and the trapped electron is somewhat less than 1 nm, the electrostatic attraction will be greater than the binding energy of the proton, and thus it is energetically possible that the proton will

move to the trapped electron and break the weak Si-Si bond. This event creates a new Si-H bond and two separated dangling bonds.

The end state is similar to that hypothesized by Dersch et al [15], but they hypothesized that the defect was created by a recombination event breaking the weak Si-Si bond and then the nearby hydrogen atom moving to the broken bond. This mechanism requires a significant amount of energy since the weak Si-Si bond must first be broken and then the Si-H bond must be broken. This mechanism is likely to require two recombination events near the complex within a very short period of time (the hydrogen atom must move before the broken Si-Si bond reforms). We believe that a much more likely event is the trapping of photogenerated charge at the complex and the subsequent motion of the proton to the trapped electron on the weak Si-Si bond.

Once the metastable defect is formed, the reverse effect could occur. That is, photogenerated carriers could be trapped at the metastable complex, and proton motion could restore the ground state. If a strong electric field is imposed on the a-Si:H during illumination, the electrons and holes will spend less time in the traps, and recombination will be reduced. However, when a hole is trapped at the Si-H bond in a metastable complex, the field could induce the proton to hop back to the ground state. Thus, the events creating metastable centers will be suppressed by the short residence times of both electrons and holes in complexes in the ground state when a strong electric field is present, but the reversal of the metastable defects to the ground state could occur whenever a hole is localized on the Si-H bond in a metastable center.

The field dependence of the recovery process supports the hypothesis of proton motion. Fig. 4.8 shows the effect of the electric field on the recovery time for a degraded cell annealed at 100^0C in the dark at various biases. The data is interpreted in terms of the Poole effect [17] where the applied field lowers the barrier for proton motion between overlapping potential wells. In this model, the activation energy is lowered by a term $e\varepsilon b/2$ where ε is the internal electric field [9], and b is the distance between potential wells. Therefore, the recovery time should follow the expression:

$$\tau_{REC} \propto \exp\{[E_a - e\varepsilon b/2]/kT\} \qquad (4\text{-}1)$$

If the potential wells are not overlapping, then the barrier lowering term becomes $e\beta\varepsilon^{1/2}$ (the Poole-Frenkel effect) where $\beta = (e/\pi\epsilon)^{1/2}$ and ϵ is the permittivity.

Analyses of the field dependence at 60^0C and at 100^0C in the dark showed that the Poole effect provides a much better fit to the data than the Poole-Frenkel effect, and a jump distance of ~ 0.9 nm was estimated from the data at both temperatures. A similar analysis of the field dependence of the recovery time for a degraded cell exposed to 50 suns at 100^0C also showed a very good fit to Eqn. 4-1, and in this case the jump distance in this case was estimated to be ~ 0.6 nm. A similar jump distance (~ 0.6 nm) was estimated for proton motion in p-i-n cells exposed to intense illumination and strong reverse biases at elevated temperatures [9]. Under those circumstances, the short wavelength response of the cells degraded as a result of the long-range motion of protons near the p/i interface.

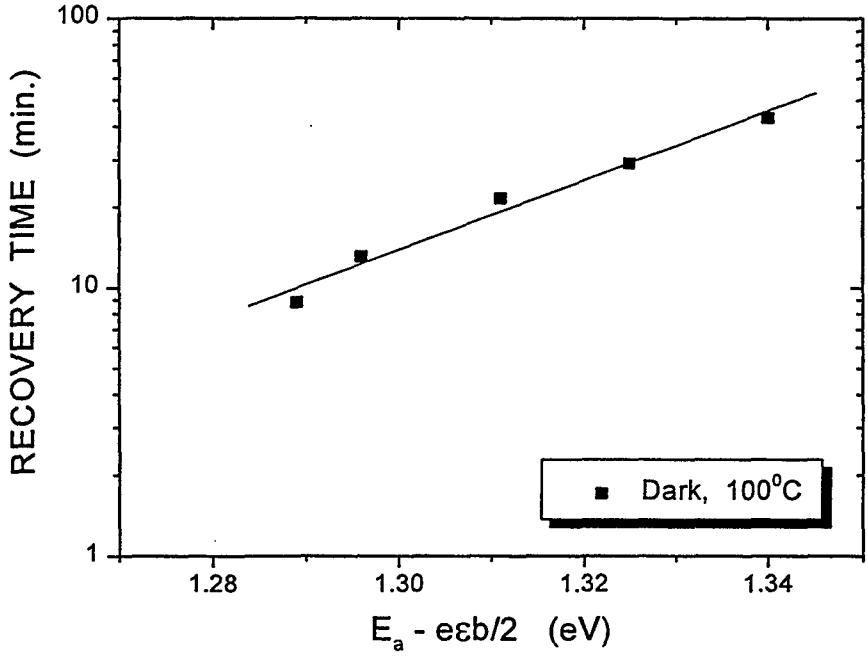

Fig. 4.8 A semi-logarithmic plot of the recovery time as a function of the field-lowered activation energy.

4.1.2 Irreversible Light-Induced Degradation in a-Si:H Solar Cells

The light-induced degradation of amorphous silicon (a-Si:H) solar cells is usually considered to be totally reversible so that the initial performance can be restored by annealing the cells for about 1 hour at temperatures of ~ 170 to 200^{0}C. An earlier study [6] showed that a small amount of the degradation induced by prolonged exposure to intense illumination at normal operating temperatures was irreversible. In that work a p-i-n cell was exposed to 60 suns illumination for 71 hours at 60^{0}C under open-circuit conditions, and some permanent loss in performance was noted even after annealing at 170^{0}C for times up to 22 hours.

The objective of the present study was to carefully measure the effects of prolonged intense illumination on a-Si:H p-i-n solar cells to determine the physical mechanisms responsible for the irreversible light-induced degradation. In one series of experiments, a p-i-n cell was exposed to 50 suns illumination at 60^{0}C for 30 minutes and was then annealed for 20 minutes at 170^{0}C. This cycle was repeated 15 times, and the photovoltaic characteristics were measured after each treatment. As shown in Fig. 4.9, the fill factor in the annealed state decreased gradually over the first several cycles, and there was also a small increase in the fill factor in the light-soaked state over the first several cycles. The short-wavelength spectral response also decreased over the first several cycles. This degradation could be reduced significantly by changing the hydrogen dilution conditions during the deposition of the p/i interface region.

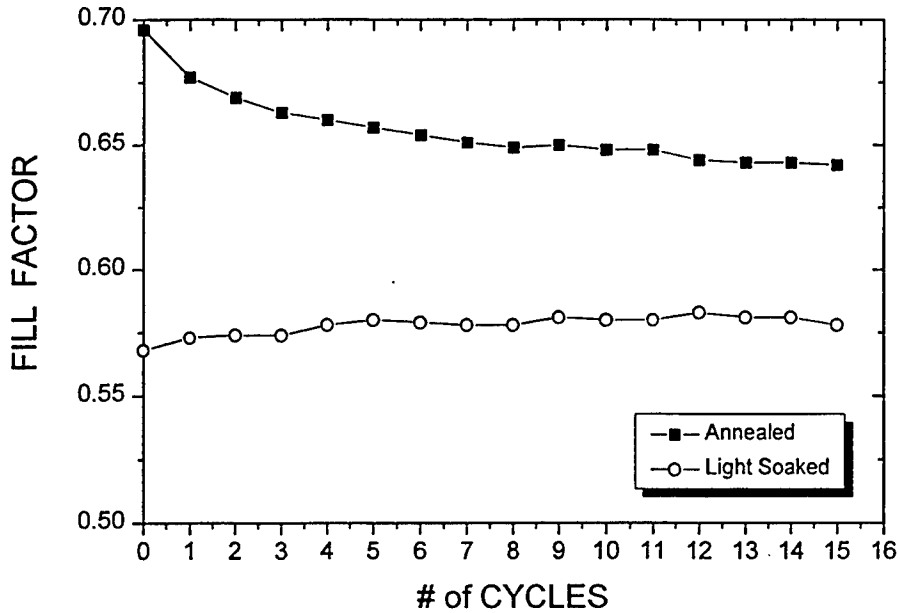

Fig. 4.9 The variation of the fill factor of a p-i-n cell with repeated cycling between an exposure to 50 suns at 60^{0}C for 30 min. and annealing for 20 min. at 170^{0}C in the dark.

In another experiment, a p-i-n cell was exposed to 60 suns at 80^{0}C for 30 hours at - 6 V reverse bias and was then annealed for 15 min. at 170^{0}C. The application of a strong reverse bias during illumination should suppress the recombination of photogenerated carriers and thus prevent light-induced degradation. However, some degradation of the photovoltaic characteristics did occur as shown in Fig. 4.10. There was a significant decrease in the short wavelength region of the spectral response after 30 hours at 60 suns at - 6 V reverse bias. The decrease in the quantum efficiency at 420 nm with time is shown in Fig. 4.11 for another p-i-n cell that was exposed to 60 suns at - 6 V for more than 100 hours at 80^{0}C. Most of this degradation could be removed by annealing the cell for 15 min. at 170^{0}C, but as shown in Fig. 4.10 there is still some loss in the short-wavelength response. Similar effects were also observed in p-i-n cells that were exposed to 1 sun illumination under a strong reverse bias for several hundred hours.

The other photovoltaic characteristics exhibited a more complicated behavior. As shown in Fig. 4.12 both the open-circuit voltage and the fill factor increased gradually with exposure to 60 suns at - 6 V while the short-circuit current gradually decreased. However, both parameters returned to their initial values when the cells were annealed for 15 min. at 170^{0}C.

A similar effect was observed when p-i-n cells were exposed to intense blue light while under a strong reverse bias. The blue light was obtained by using the Xe arc lamp in conjunction with a filter that transmitted light with wavelengths between 420 and 460 nm.

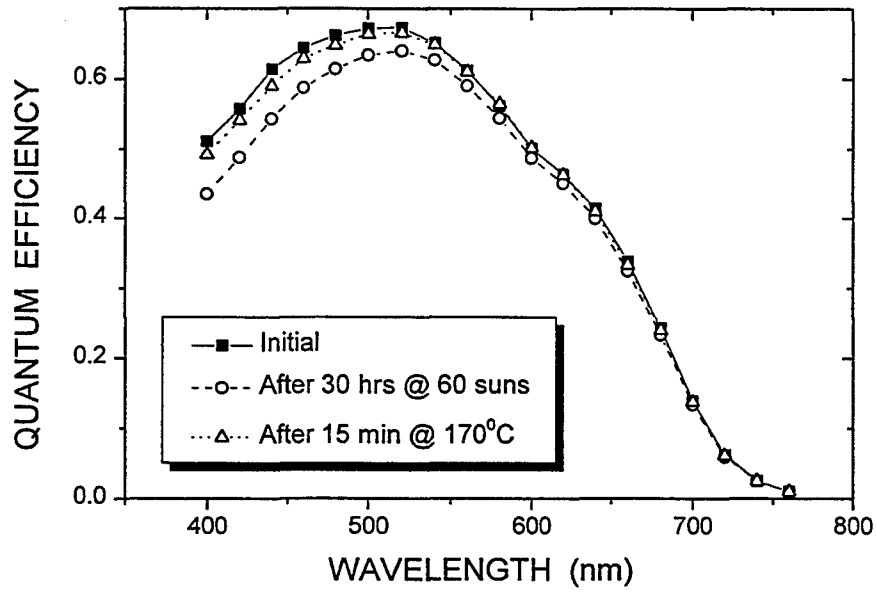

Fig. 4.10 The spectral response of a p-i-n cell that was exposed to 60 suns for 30 hours at - 6 V reverse bias and was then annealed for 15 min. at 170^{0}C.

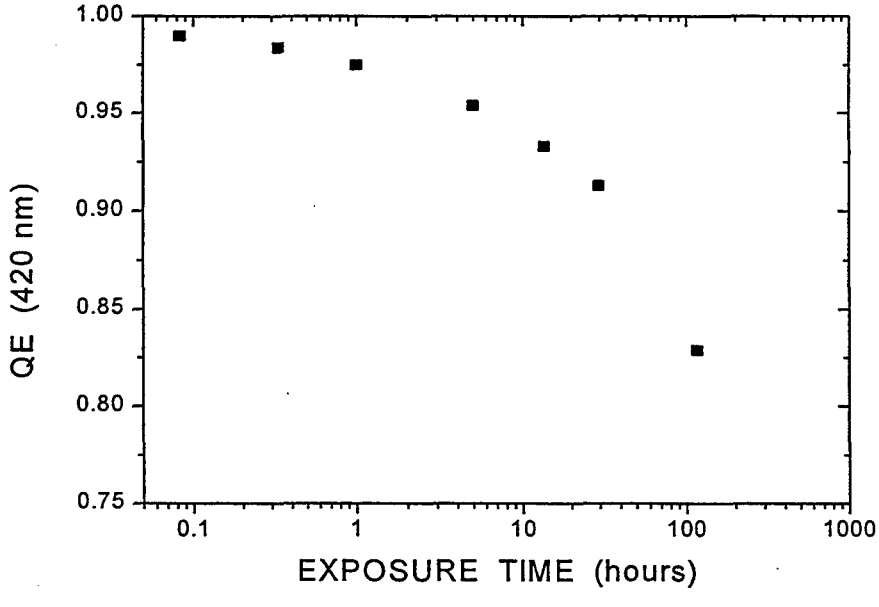

Fig. 4.11 The quantum efficiency at 420 nm vs. time for a p-i-n cell exposed to 60 suns at 80^{0}C at - 6 V reverse bias.

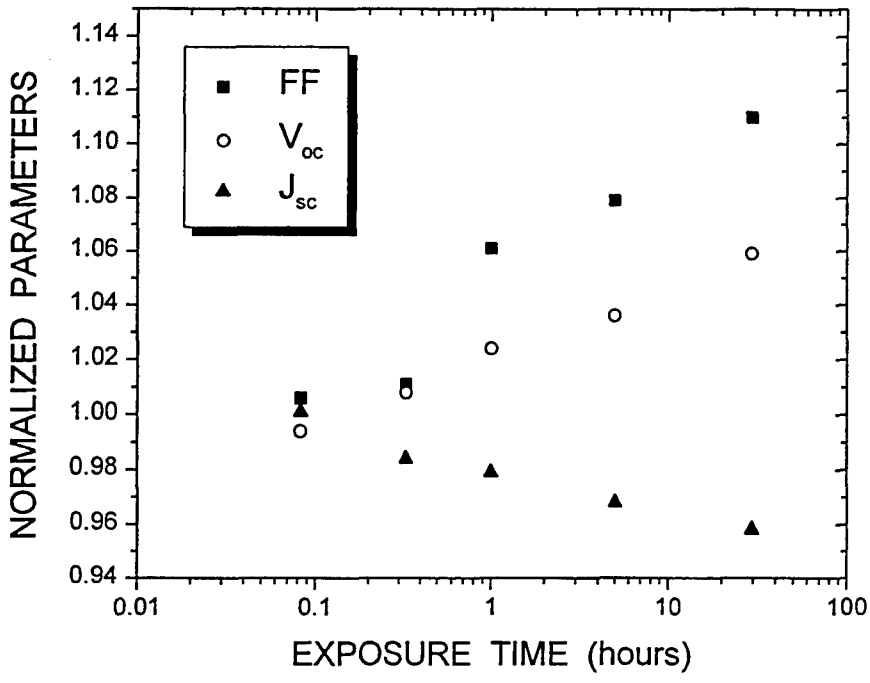

Fig. 4.12 The variation of the normalized fill factor, open-circuit voltage and short-circuit current density vs. time for a p-i-n cell exposed to 60 suns at - 6 V reverse bias.

The data in Fig. 4.13 show that the conversion efficiency improved rapidly in the first few minutes of exposure and the rate of improvement exhibited only a weak temperature dependence. The conversion efficiency increased due to increases in both V_{OC} and FF while J_{SC} showed a slight decrease. The same cells were also subjected to the same reverse bias (- 9 V) at elevated temperatures in the dark; this reverse bias annealing treatment is described in reference 18. As shown in Fig. 4.14 the conversion efficiency exhibited similar improvements, but much higher temperatures were required, and the effect is now strongly temperature dependent. If we define a characteristic rise time as the time that it takes for the conversion efficiency to improve by 9%, and then plot this characteristic time on an Arrhenius plot, then the activation energies obtained from the data in Figs. 4.13 and 4.14 are ~ 0.23 and ~ 1.15 eV, respectively.

The data presented in this section can be interpreted in terms of hydrogen motion in the vicinity of the p/i interface. Earlier work [9] showed that protons could be induced to move in a-Si:H at elevated temperatures in the presence of intense illumination and strong reverse biases. The irreversible degradation of the short-wavelength spectral response and the reversible improvements in V_{OC} and the FF may both be due to proton motion that occurs even at normal operating temperatures when both intense illumination and strong electric fields are present.

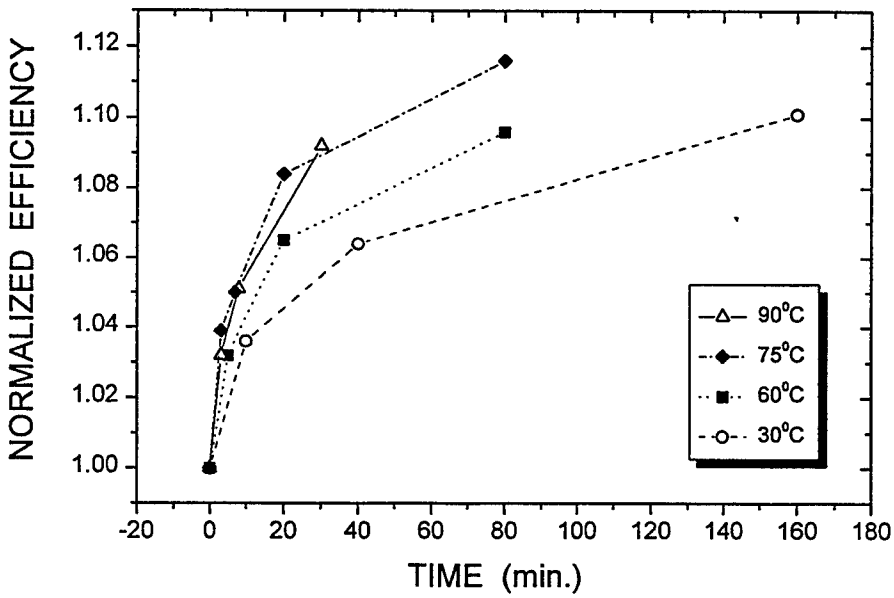

Fig. 4.13 The normalized conversion efficiency vs. time for p-i-n cells exposed to blue light (3.5 x J_{SC}) at - 9 V reverse bias at various temperatures.

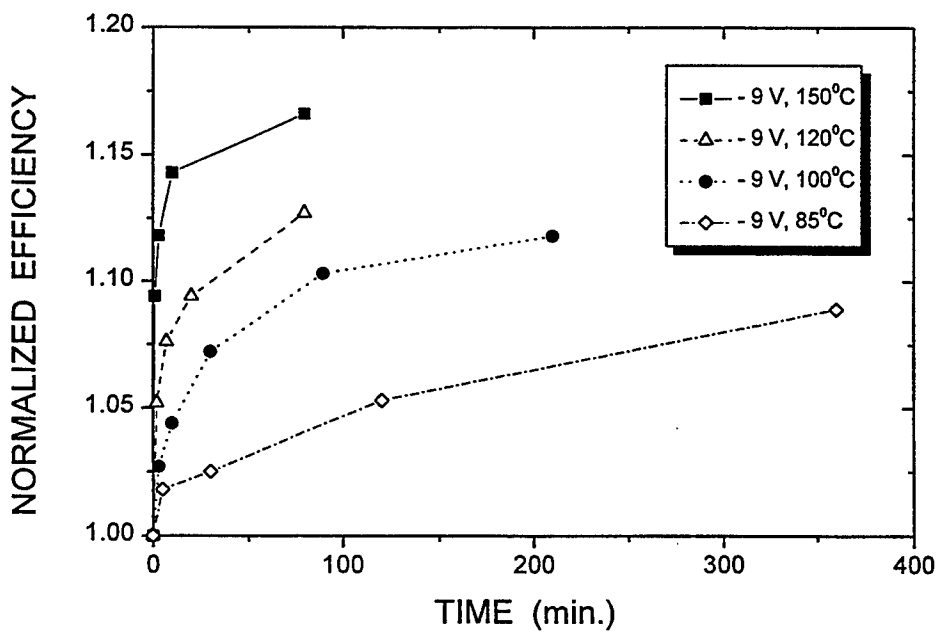

Fig. 4.14 The normalized conversion efficiency vs. time for p-i-n cells annealed in the dark at -9V reverse bias at various temperatures.

4.1.3 The effect of light-soaking on reverse-biased annealed cells

As mentioned in the previous section, we have observed that both the open-circuit voltage and the fill factor of a-Si:H p-i-n cells can be improved by exposing the cells to intense illumination under a strong reverse bias at normal operating temperatures (~ 40 - 70^{0}C). This process appears to be very similar to reverse bias annealing in the dark at higher temperatures (~ 150 - 180^{0}C), but the activation energy is only about 0.23 eV for the illuminated reverse bias treatment as compared to about 1.15 eV for reverse bias annealing in the dark. The improvement of the photovoltaic properties after reverse bias annealing may be due to the activation of acceptor sites as protons are field-driven away from passivated boron atoms. Under intense illumination, the protons may be able to move by thermally assisted tunneling, thus accounting for the low activation energy.

We made some p-i-n devices with deuterated p/i regions by using SiD_4 and deuterated diborane (B_2D_6). Both the deuterated cells and conventional p-i-n cells were subjected to reverse bias annealing in the dark and were then exposed to 1 sun illumination for several hundred hours. All cells exhibited an improvement in performance upon reverse bias annealing, but the improvements disappeared after prolonged illumination. These observations appear to rule out thermally assisted tunneling of protons as a mechanism that would allow hydrogen to move under illumination at normal operating temperatures. If tunneling mechanisms were responsible for the loss of the enhanced V_{OC} and FF values with light soaking, then the replacement of hydrogen with deuterium should make the enhancements insensitive to light soaking.

In the course of these studies, we did find that the results depend on the deposition conditions used to form the junction. In most cases, the improvements in conversion efficiency are lost when the p-i-n cells are exposed to 1 sun illumination for several days (see Fig. 4.15).

However, some p-i-n cells were able to retain the relative improvements caused by reverse bias treatments for longer periods of light soaking as shown in Fig. 4.16. In this case, the p-layer was lightly doped so that it was fully depleted, and both V_{OC} and FF were somewhat less than the standard cells, but J_{SC} was larger. As is evident from the data in Fig. 4.16 the performance of these cells was improved significantly after a reverse bias treatment in the dark at 180^{0}C, and a small increase in performance is evident even after 660 hours of 1 sun illumination. However, a comparison of the data in Figs. 4.15 and 4.16 shows that the cells with depleted p-layers degraded faster than the control cells with normal p-layers.

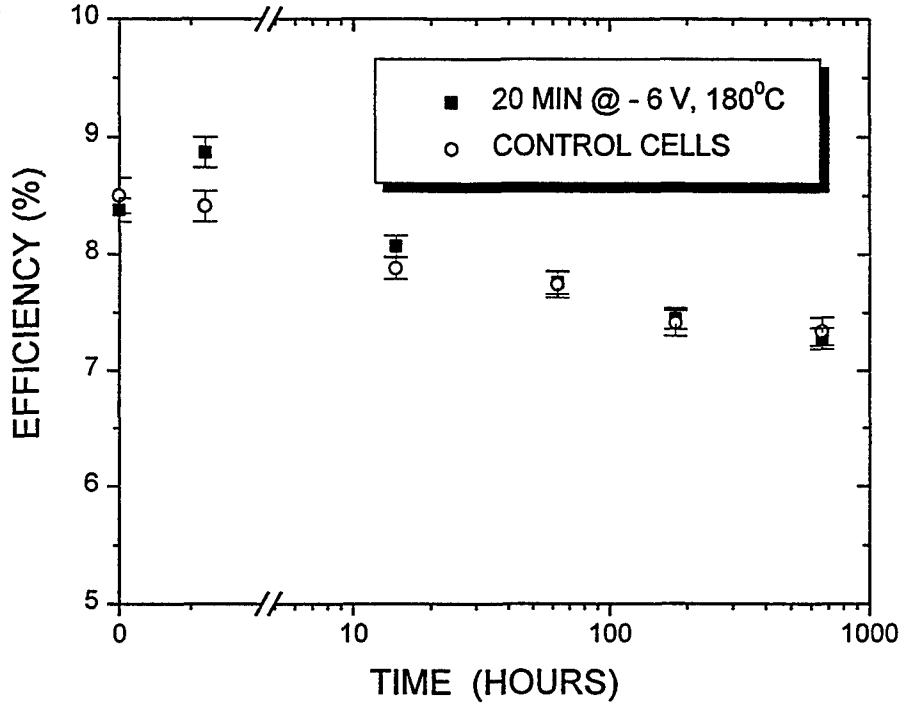

Fig. 4.15 The conversion efficiency of standard p-i-n cells as a function of time exposed to 1 sun illumination.

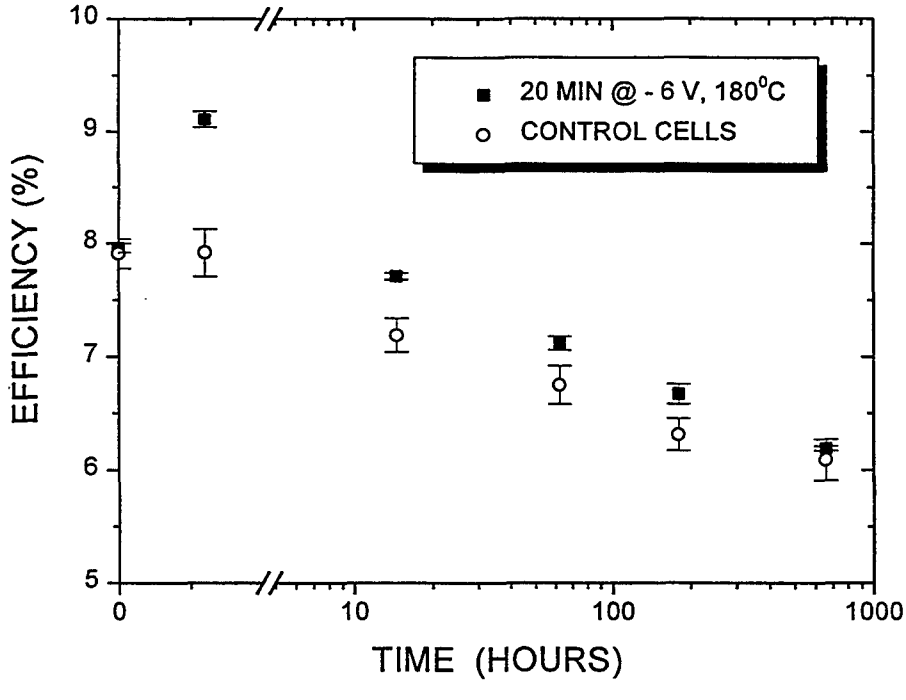

Fig. 4.16 The conversion efficiency of p-i-n cells with a depleted p-layer as a function of time exposed to 1 sun illumination.

4.1.4 Study of the amorphous silicon / tin oxide interface

Contamination at the interface between the amorphous silicon p-layer and the tin oxide coated glass can strongly affect the performance of amorphous silicon solar cells. We find that some commercially available TCO (transparent conductive oxide) coated glass often has a thin layer of some residual materials on the surface even after our normal cleaning process.

There are several materials that are commonly used in shipping commercial TCO coated glass: sulfur trioxide to protect the glass from scuffs and scratches, malic acid as an anti-staining agent and to prevent corrosion of the glass, polypropylene beads to keep the glass pieces from sticking together, and anhydrous adipic acid as an anti-staining agent.

Adipic acid is only weakly soluble in water at low temperatures. In the current cleaning process, the TCO coated glass is cleaned using a commercial glass washing machine. The temperature in the detergent tank of the washer is about 66^0C, and the temperature of the rinse water is about 20^0C. Thus, because of its poor solubility at these temperatures, some residual adipic acid appears to be left on the TCO surface after cleaning in the commercial washer. This residual adipic acid appears to be introducing a resistive layer with a series resistance of about 2 ohm-cm^2 into the solar cell structure.

A series of cleaning experiments were performed using single-junction a-Si:H solar cells, and the results are summarized in Table 4.1 where we show typical values of the open circuit voltage, fill factor and series resistance for cells cleaned with three different techniques. We found that the best method to remove the contaminant layer is to use an ultrasonic cleaning process with a heated detergent solution followed by a rinse in de-ionized water.

Table 4.1 Solar Cell Performance Using Different Cleaning Processes

Cleaning Processes	V_{oc} *(V)*	*Fill Factor*	R_S *(ohm-cm^2)*
Normal Cleaning Process	0.88-0.90	0.63-0.67	7.6 - 9.0
Ultrasonic Method	0.91-0.93	0.69-0.72	6.1 - 7.2
Lye Bath Process	0.91-0.92	0.69-0.70	6.6 - 7.4

An adipic acid layer can also be removed by rinsing the TCO coated glass in a hot lye bath. After rinsing with de-ionized water, the glass was then passed through the Billco washer. As shown in Table 4.1, the performance of the cells cleaned in the lye bath was close to that obtained with the ultrasonic cleaner.

A number of experiments were performed to try to improve the efficacy of the commercial washer. We tried reducing the speed of the washer, increasing the temperature of the detergent solution, rinsing the TCO coated glass with hot water, using high pressure steam to rinse the TCO coated glass, adding a small amount of NaOH into the detergent solution to increase its pH value, and using a new detergent. However, the solar cell performance did not improve significantly with any of these methods. Thus, the ultrasonic cleaning procedure is currently the best way to clean commercial TCO coated glass.

4.1.5 Improvement of Gas Utilization

The cost of manufacturing thin film PV modules can be reduced by increasing the stabilized efficiency, increasing the throughput or by reducing the feedstock material. In this part of the report, we will discuss the experiments performed to reduce the feedstock cost in our deposition process.

The p-i-n cells used in this study had a structure of Glass / SnO_2 / SiC p-layer / a-Si:H i-layer / n-layer / ZnO / Al. No changes were made to the p- and n-layers during this study, and hydrogen-diluted silane was used in all the i-layers. The thickness of the i-layers was kept at ~ 300 nm throughout the study. A series of cells were made by starting with our control cell deposition conditions and then systematically lowering the total gas flow during the i-layer deposition. The growth rate remained roughly constant for all the samples except for the very low flow rate samples. With the lowest flow rate, we were able to triple the gas utilization as compared to our standard conditions. The measured characteristics are given in Table 4.2. The open-circuit voltages of these devices steadily increased with decreasing flow while the short-circuit current showed a corresponding decrease. The loss in short-circuit current could be mainly attributed to the lowering of the blue response in the spectral response measurements. There was very minimal voltage bias dependence of the spectral response for these samples which eliminates the possibility of boron contamination of the i-layer. We think that, depending on the flow conditions we used, the conditions were different at the beginning of the i-layer deposition, which may resulted in an increase in V_{OC} and a lowering of the blue response.

Table 4.2 Varying the Flow Rates for the Deposition of the i-Layer in p-i-n Cells

Sample #	*I - layer flows*	*V_{OC} (V)*	*FF*	*Rs ($ohm\text{-}cm^2$)*	*J_{SC} (mA/cm^2)*	*QE(400)*	*Thickness (nm)*
L6240-2	Control	0.864	0.696	5.84	13.81	0.574	320
L6241-1	50% lower	0.875	0.642	8.98	13.27	0.533	
L6241-2	75% lower	0.919	0.671	6.83	11.35	0.376	
L6241-3	90% lower	0.951	0.679	10.6	9.61	0.274	290

These results led us to look at the p-layer and p/i buffer layer deposition conditions more closely in order to better understand the initial growth of the i-layer on top of the p-layer. In one deposition system we varied the flush time and the flow rate at the beginning of the i-layer (see Table 4.3). As long as we maintained either high flow rates during the flush cycle or had a thin buffer layer with high flow rates followed by a low flow rate i-layer, we were able to get the high blue response along with open-circuit voltages of ~ 0.870 V. Increasing the flush time had minimal effect on both those characteristics. SIMS data also showed more hydrogen in the i-layer of the low flow samples.

Table 4.3 Varying Flush and Deposition Flow Rates

Sample	*Flush Flows for Buffer Layer*	*Dep. Flows for Buffer Layer*	*Flush Flows for i-layer*	*V_{OC} (V)*	*FF*	*J_{SC} (QE)*	*QE (400nm)*
L6240-2	none	none	Control	0.864	0.696	13.81	0.57
L6241-3	none	none	90% lower	0.951	0.679	9.61	0.274
L6242-3	none	none	90% lower	0.953	0.73	10.44	0.37
L6242-3	50% lower	50% to 90% lower	90% lower	0.873	0.713	12.7	0.64
L6243-2	50% lower	50% to 90% lower	90% lower	0.863	0.713	12.45	0.654
L6243-3	none	none	50% lower	0.88	0.698	12.8	0.638

In another deposition system (a multi-chamber system) we repeated the experiments with the two extreme total flow conditions (see Table 4.4). In this deposition system, different hydrogen dilution conditions were used in the vicinity of the p/i interface. In these samples we did not see the drop in the blue response or the increase in the V_{OC} as we saw in our first study. Both the cells had nearly the same performance. This result strongly suggests that the p/i interface deposition conditions plays a major role in the overall performance of these cells. The intentional hydrogen treatment of the interface also increases the open-circuit voltage and fill factor. Thus, by optimizing the hydrogen content at the interface, we may be able to maintain the same cell performance while conserving the feedstock during the i-layer deposition.

Table 4.4 M-System Low Flow Samples (p-i-n, no p/i buffer)

Sample	*I - layer*	*Voc*	*FF*	*Rs (ohm-cm^2)*	*Jsc (QE)*	*Thickness*
M7084-3-2	Control	0.868	0.707	4.53	13.58	3000
M7084-4-2	75% lower	0.876	0.72	5.4	13.94	3000

A series of experiment were conducted in another deposition system. When the silane flow was reduced by a factor of two from our normal deposition conditions, the initial performance and stability of the cells were essentially unchanged, and the deposition rate was reduced by only about 10%. Reducing the silane flow by a factor of four caused the deposition rate to drop by 25% while the initial and final performance were essentially the same as that of the control cells. This observation shows that at when we reduce the silane flow by a factor of four, we are getting close to the depletion regime. We were able to obtain excellent uniformity for films deposited on 1 ft^2 substrates even at these reduced silane flow rates with a 10:1 hydrogen dilution ratio. By increasing the plasma power and/or lowering the hydrogen dilution ratio, we were able to almost double the deposition rate with no loss in performance. These results are summarized in Table 4.5. The differences in the light-induced degradation are most likely largely due to the differences in the thickness of the cells.

Table 4.5 Summary of Silane Flow Experiments in the A-system

Sample Number	*Norm. Discharge Current*	*Norm. H2 flow*	*Norm. Silane flow*	*Thick. (nm)*	*Norm. Dep. Rate*	*Norm. Utiliz.*	*Voc (V)*	*FF*	*Eff. Degr. (%)*
A7127-1	1	1	1	310	1	1	0.91	0.72	36
A7127-2	1	0.5	0.5	270	0.87	1.74	0.93	0.72	32
A7128-1	1	0.25	0.25	220	0.73	2.95	0.92	0.71	25
A7134-2	1	0.35	0.5	368	1.19	2.36	0.91	0.72	39
A7135-3	1.67	0.5	0.5	440	1.43	2.83	0.91	0.71	39

We fabricated a-Si:H cells in a single-chamber system using lower silane flow rates with both hydrogen and helium dilution of silane. In Table 4.6 we show the initial and stabilized performance of a few cells prepared with a 50% reduction in the silane flow compared to our standard cells. The data in Table 4.6 show that stabilized performance of the cells fabricated under improved gas utilization is nearly same as our control cells.

Table 4.6 Performance of a-Si:H cells with hydrogen and Helium diluted i-layers prepared in the C-system

Run #	*Diln. Ratio*	*Rel. Silane Flow*	*FF*	*Jsc (QE) (mA/cm^2)*	*Eff. (%)*	*Stabilized Eff.*	*Degradation in Eff.(%)*
Std. He	10:1 (He)	1	0.714	14.7	9.6	7.47	22.2
C7302-3	20:1 (He)	0.5	0.718	13.8	9.1	7.22	21.5
C7307-2	20:1 (He)	0.5	0.71	14.0	9.1	6.94	24
C7316-5	20:1 (He)	0.5	0.704	13.9	9.0	6.84	24
Std. (H_2)	10:1 (H_2)	1	0.712	14.3	9.5	7.27	23
C7317-5	20:1 (H_2)	0.5	0.725	12.6	8.3	6.83	17.7
C7318-3	20:1 (H_2)	0.5	0.724	13.0	8.5	6.9	19.1
C7318-4	20:1 (H_2)	0.5	0.70	14.1	8.9	7.57	14.9

Reducing gas flows leads directly to reduced materials costs, but there is also substantial cost benefit if we add on the additional cost savings from the reduced scrubber maintenance and the reduction in the time required for cleaning the deposition systems.

4.1.6 Comparison of Growth Processes Using Hydrogen and Helium Dilution

The growth of a-Si:H comprises several processes: silane decomposition, gas phase reactions and surface reactions. We did a comparative study of feedstock dissociation using both hydrogen and helium-diluted discharges and measured the activation energies of surface reactions by comparing the deposition rates under different conditions.

The variation of the deposition rate (R_d) of H- and He-diluted a-Si:H with silane flow is shown in Fig. 4.17 and Fig. 4.18. The data show that the deposition rates increase with silane flow and are higher for He-dilution than for H-dilution (all other deposition conditions were similar). A comparison of the data in Figs. 4.18 and 4.17 shows that the difference between the deposition rates for helium and hydrogen dilution is greater when the discharge power is lower.

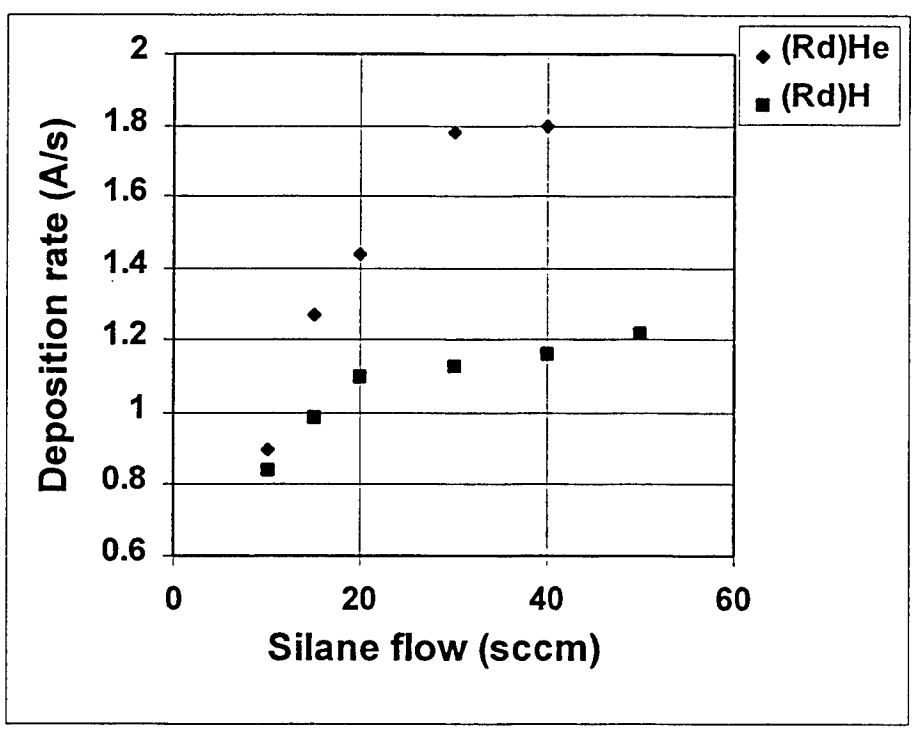

Fig. 4.17 Effect of silane flow on the deposition rate for a-Si:H films grown in H- and He-diluted (10:1) discharges (normalized discharge current = 1).

These observations lead us to conclude that helium dilution increases the decomposition of undissociated silane molecules. It is well known that long lifetime metastable helium atoms (He^*) with excitation energies of ~ 20 eV are generated in the helium discharge. On de-excitation (by collision with a silane molecule), the energy of the excited helium atom may be sufficient to decompose the undissociated feedstock. Fig. 4.19 represents same as Fig. 4.17, the only difference is that a-Si:H films have been deposited under higher dilution (20:1). A comparison of Figs. 4.17 and Fig. 4.19 reveals that the increase in R_d when hydrogen is

replaced by helium (for a constant silane flow) is greater at the lower dilution (10:1). For example, for a silane flow of 20 sccm, the % increase in R_d is 31 and 55 % for 10:1 and 20:1 dilution, respectively when hydrogen is replaced with helium. As the dilution ratio of helium to silane is increased, the concentration of He^* in the discharge increases. These results support the hypothesis that He^* is taking part in effectively decomposing undissociated process gas. Thus helium dilution appears to be an effective approach to improving the utilization of feedstock gases.

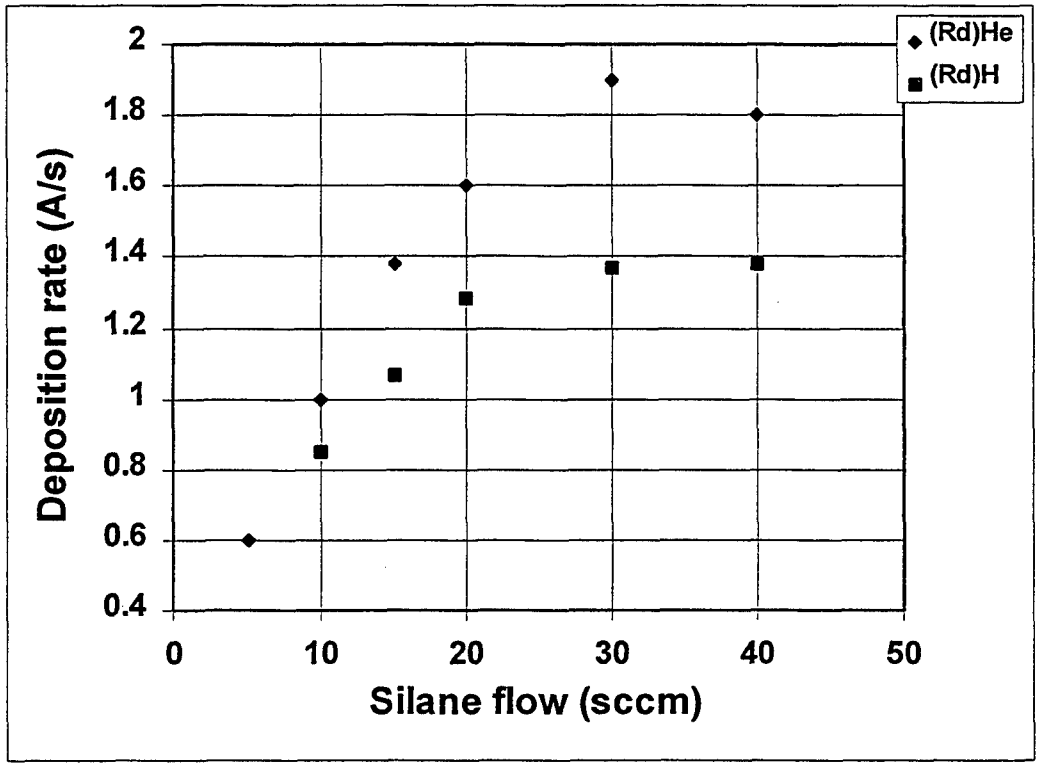

Fig. 4.18 Deposition rate vs. silane flow for a-Si:H films grown in H- and He-diluted (10:1) discharges (normalized discharge current = 1.12).

Since the growth of a-Si:H is due to the interaction of a plasma and a solid growing film surface in a non-equilibrium condition, the surface reactions during film growth are a vital step in determining the network structure and the defect structure of the resulting film. To elucidate the growth mechanisms, we compared the temperature dependence of R_d under two different discharge conditions. The data in Figs. 4.20 and 4.21 show the temperature dependence of R_d for H- and He-diluted a-Si:H films deposited at dilution ratios of 10:1 and 20:1 respectively.

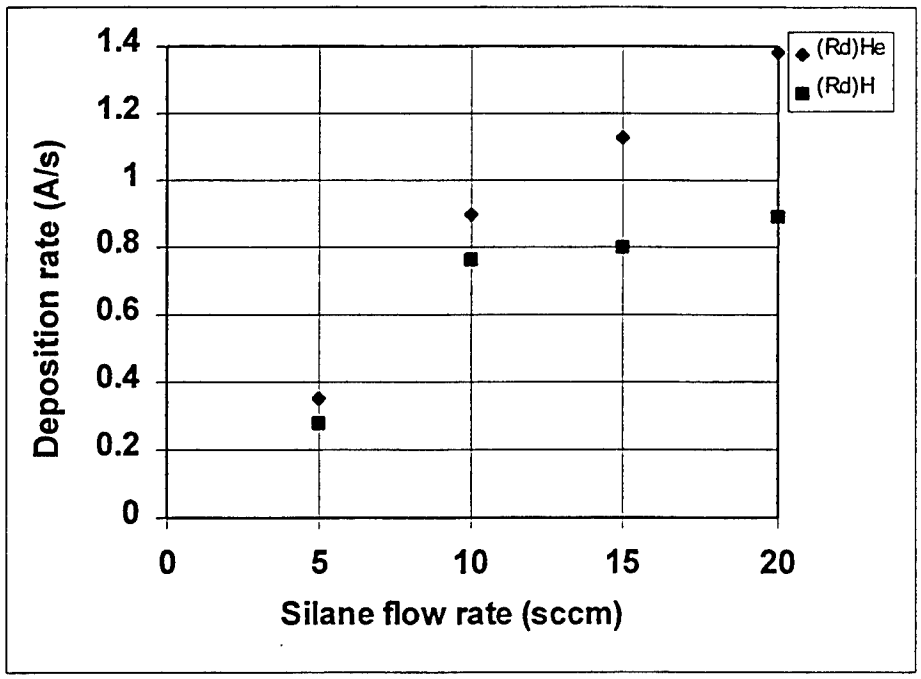

Fig. 4.19 Deposition rate vs. silane flow for a-Si:H films grown in H- and He-diluted (20:1) discharges (normalized discharge current = 1).

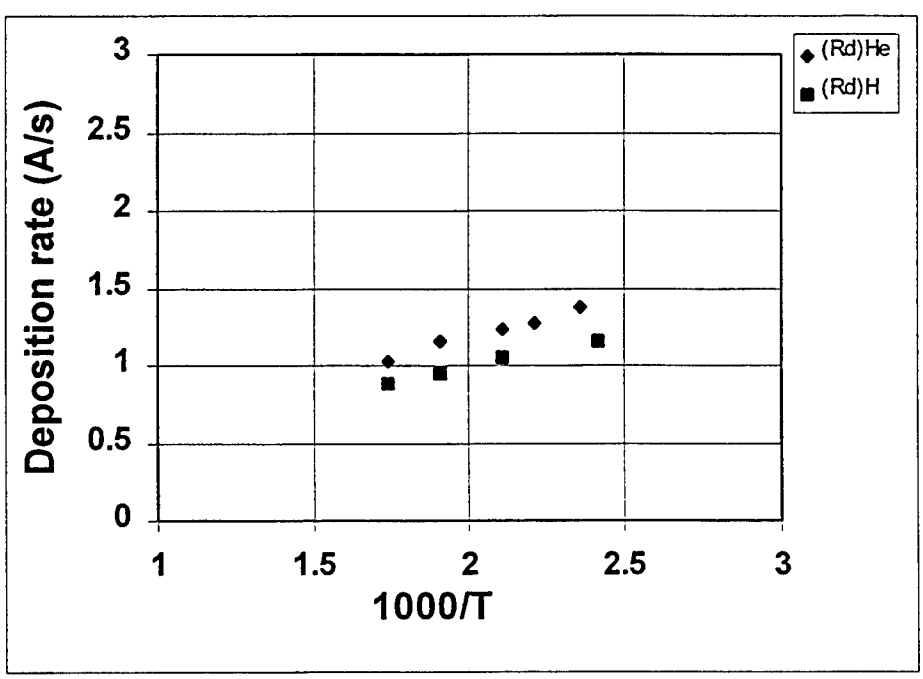

Fig. 4.20 Deposition rate vs. inverse temperature for a-Si:H films grown in H- and He-diluted (10:1) discharges.

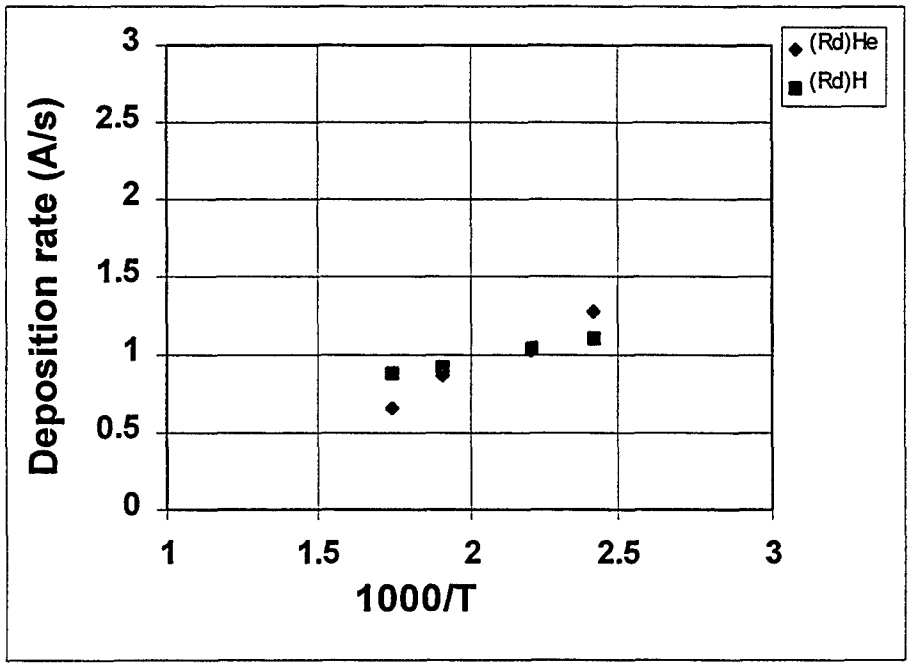

Fig. 4.21 Deposition rate vs. inverse temperature for a-Si:H films grown in H- and He-diluted (20:1) discharges.

In the case of a 10:1 dilution, the deposition rate is a weak function of temperature for both H- and He-diluted films, and the activation energy is somewhat greater for the He-diluted materials. When the dilution is increased from 10:1 to 20:1, the activation energy for the surface growth of the H-diluted films remains unchanged whereas it increases significantly for the He-diluted materials (see Fig. 4.21). It should be mentioned that the deposition rate has been found to be almost independent of substrate temperature over the range of 100 to 300°C for a-Si:H films grown using RF PECVD with helium dilution [19]. It is not clear why our a-Si:H films grown in a DC PECVD mode with helium dilution exhibit a significant temperature dependence especially at a 20:1 dilution.

When excited He^* atoms interact with silane molecules, the excess energy not only helps to dissociate the silane, but also increases the kinetic energy of the decomposed species, thus enhancing the surface mobility of the precursors (SiH_3, SiH_2 etc). The extra energy supplied to the matrix can modify the network structure and hence the properties of the a-Si:H films. This hypothesis has been corroborated by the fact that both the hydrogen content and the concentration of microstructural defects (polyhydride and microvoids) are significantly lower in the case of He-diluted a-Si:H than for H-diluted materials. (Thus, it appears as though the He-diluted films were grown at a higher substrate temperature [20]). Other work has shown that the hydrogen content of a-Si:H films grown by the layer-by-layer technique can be significantly decreased by treating the growing layers with He^* rather than with atomic hydrogen [21].

4.1.7 Comparison of Light-Induced Degradation of Hydrogen- and Helium- Diluted Amorphous Silicon Solar Cells

We have been investigating amorphous silicon (a-Si:H) and amorphous silicon germanium alloys (a-SiGe:H) deposited using helium dilution in order to overcome two major drawbacks of commonly used hydrogen dilution technology; i.e. low growth rate and low feedstock utilization. We reported in the previous section that the silane utilization could be improved by 50% by taking advantage of the higher electron temperature (plasma energy) of the He-diluted discharge. In some recent experiments, we compared the degradation kinetics of single-junction cells in two H-diluted samples and one He-diluted sample. The common structure of the cells is p-type a-SiC:H / buffer / a-Si:H / n-type μc-Si:H. The initial performance of the cells is shown in table 4.7

Table 4.7 Initial PV characteristics of H- and He-diluted a-Si:H

Run # (diluent)	Thick. (nm)	Rel. R_d	$\langle V_{oc} \rangle$ (V)	<FF>	J_{sc}(QE) (mA/cm^2)	<Eff.> (QE)	Degrad. in FF (%) (1000h)	Degrad. in Eff. (%) (1000h)
C7301-1 (H)	300	1	0.902	0.712	14.3	9.2	17.2	23.4
C7301-2 (H)	299	1	0.904	0.714	14.7	9.5	17.0	23.0
C7344-1 (He)	312	1.52	0.903	0.711	14.01	9.0	16.0	23.2

It may be noted from the Table 4.7 that although the deposition rate is increased by about 52% the intrinsic layer grown with He dilution, the open circuit voltage and the fill factor of the cell in the initial state is same as that for H-diluted cells. Generally, the film quality deteriorates when the deposition rate is increased for cells made with hydrogen dilution. These results indicate that for He-diluted materials, either the effective substrate temperature is increased (since extra energy is supplied from the He discharge) or the growth mechanism is different.

In order to compare the effects of light soaking, all three samples were exposed to AM 1.5 illumination at 50°C. In Figs. 4.22 and 4.23 we show the variation of the average FF and conversion efficiency with light soaking time for six to eight cells in each case. In all three cases, the degradation exhibits a fast degradation in the first 100 hours followed by a slow degradation that tends to saturate after several hundred hours. As is evident from the data in Figs. 4.22 and 4.23 and in Table 4.7, the amount of degradation is similar for H- and He-diluted cells even though the intrinsic layer was deposited at a rate that was 52% higher in the He-diluted cells.

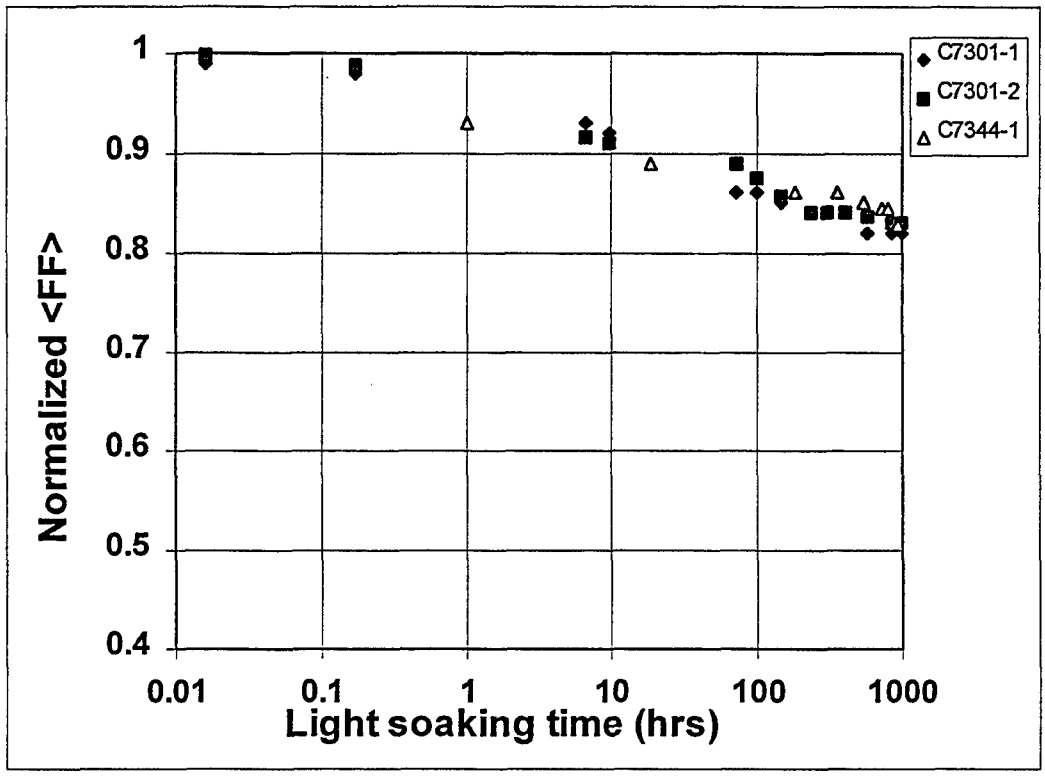

Fig. 4.22 Variation of the normalized FF with light soaking time.

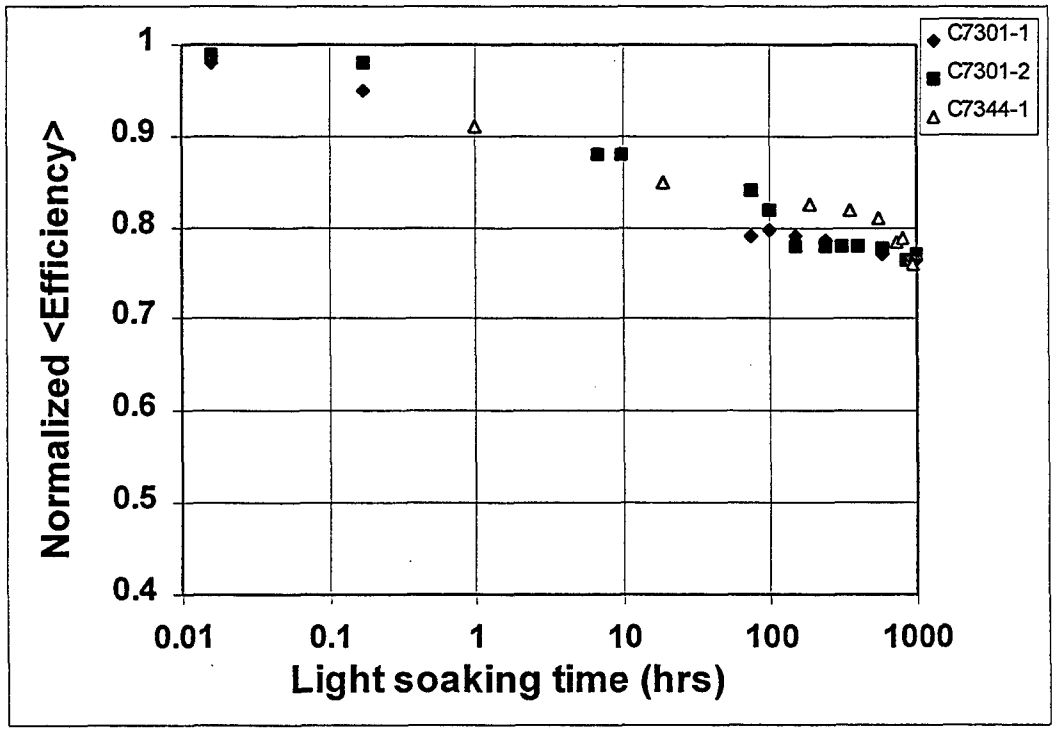

Fig. 4.23 Variation of the normalized efficiency with light soaking time.

4.2 Task 2: Low-bandgap Alloy Research

4.2.1 Field-Enhanced Recovery of Degraded a-SiGe:H Cells

Several experiments were performed to investigate the effects of strong reverse biases on the recovery of light-soaked a-SiGe:H single-junction cells. In the first set of experiments, we looked at the effects of a strong reverse bias on the annealing of degraded a-SiGe:H and a-Si:H cells in the dark at 100^{0}C. The cells were initially degraded by exposing them to 50 suns for 30 minutes at 60^{0}C under open-circuit conditions. The cells were then annealed in the dark at 100^{0}C under open-circuit conditions and at a reverse bias of - 4 V. The a-SiGe:H cell was ~ 240 nm thick while the a-Si:H cell was ~ 290 nm thick. As shown in Fig. 4.24, a reverse bias accelerates the annealing process in both a-SiGe:H and a-Si:H cells, but the recovery process both at open circuit and at - 4 V proceeds more slowly in the a-SiGe:H cells.

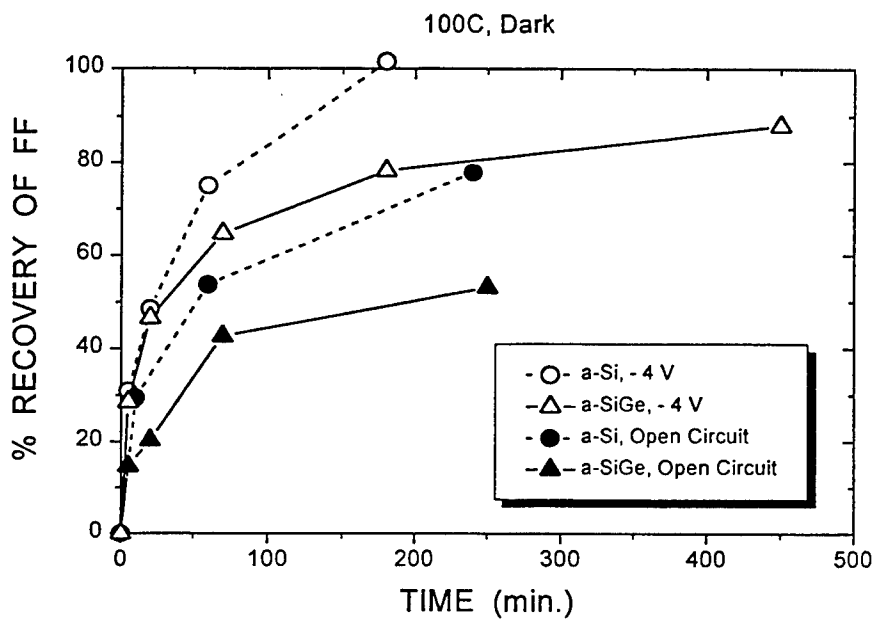

Fig. 4.24 The recovery of the fill factor of degraded a-Si:H and a-SiGe:H cells as a function of annealing time at 100^{0}C in the dark for different bias conditions.

In the second series of experiments, a-Si:H and a-SiGe:H cells were degraded by exposure to 60 suns for 30 minutes at 60^{0}C under open-circuit conditions. They were then exposed to 60 suns for 200 minutes while under a reverse bias of - 4 V at 100^{0}C. As shown in Fig. 4.25, both the a-Si:H and a-SiGe:H cells exhibit an enhanced recovery of the light-induced degradation when they are exposed to both intense illumination and strong reverse biases. As in the case of annealing in the dark, the recovery process appears to be somewhat slower for the a-SiGe:H cells. As also shown in Fig. 4.25, the recovery process is even slower for an a-Si:H cell made in a pure silane discharge. The a-Si:H cells were ~ 350 nm thick while the a-SiGe:H cell was ~ 170 nm thick. Since earlier work [11, 22] showed that the recovery process speeds up as the electric field increases, we would expect the recovery of the a-SiGe:H cell to be even slower if the thickness of the cells were all equal.

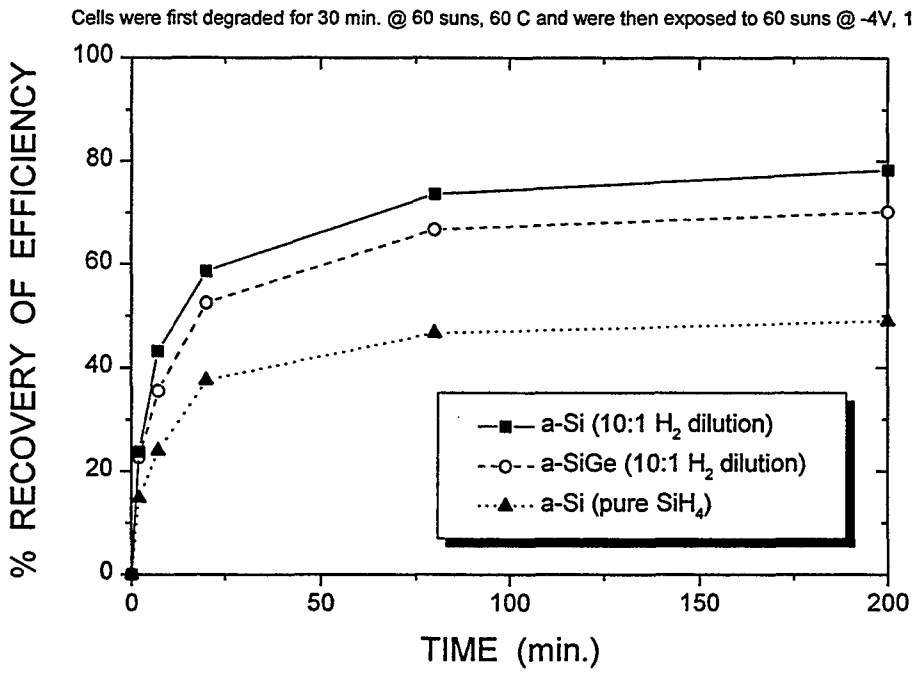

Fig. 4.25 The recovery of the efficiency of degraded a-Si:H and a-SiGe:H cells as a function of time at 100^0C while exposed to 60 suns at – 4 V.

We also looked at the relative rate of light-induced degradation in both a-Si:H and a-SiGe:H single-junction cells when exposed to intense illumination under open-circuit conditions. As shown in Fig. 4.26, the normalized conversion efficiency falls more slowly for an a-SiGe:H cell as compared to an a-Si:H cell of comparable thickness. While the a-Si:H cell degrades more rapidly in the first several minutes, the degradation tends to saturate at longer times while continued degradation is evident in the a-SiGe:H cell. When the thickness of the i-layer in the a-Si:H cell is increased, the degradation increases but the overall behavior is similar to the thinner cell.

In a third set of experiments, annealed a-Si:H and a-SiGe:H cells were subjected to intense illumination and a strong reverse bias at 220^0C. For treatment times of a few minutes, the open-circuit voltage and the fill factor increase for both a-Si:H and a-SiGe:H cells while the short-circuit current exhibits a small decrease. We attribute the increases in V_{OC} and FF to the activation of hydrogen-passivated acceptor sites in the p-layer. Similar effects are observed in the dark at temperatures of ~ 150^0C and under intense illumination at ~ 60^0C when strong reverse biases are present [23]. In all cases, we believe that the strong fields induce protons to move away from the passivated boron atoms thus electrically activating them.

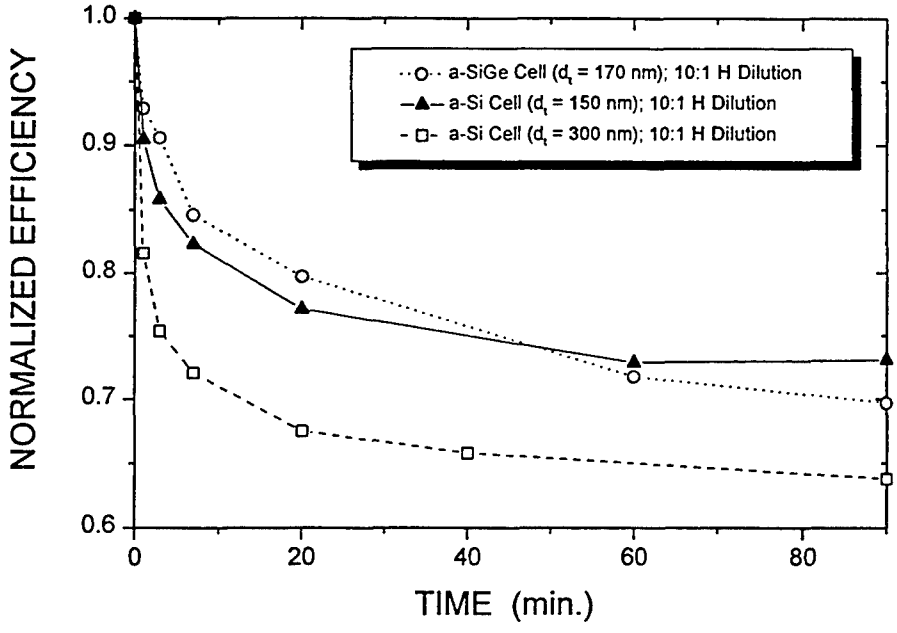

Fig. 4.26 The normalized conversion efficiency of a-Si:H and a-SiGe:H cells as a function of time exposed to 60 suns illumination at 60 °C under open circuit.

The decrease in the short-circuit current is associated with a decrease in the short wavelength spectral response as shown in Fig. 4.27 for a a-SiGe:H cell. Similar behavior is observed in a-Si:H cells as shown in Fig. 4.28. The decrease in the short wavelength response has been attributed to proton motion near the p/i interface [9].

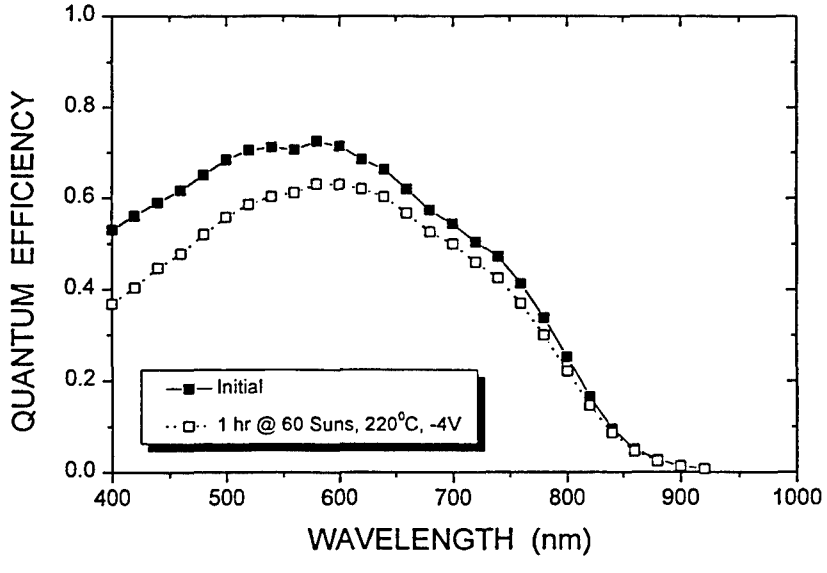

Fig. 4.27 The spectral response of an a-SiGe:H cell before and after exposure to 60 suns for 1 hour at 220^0C at a reverse bias of - 4 V.

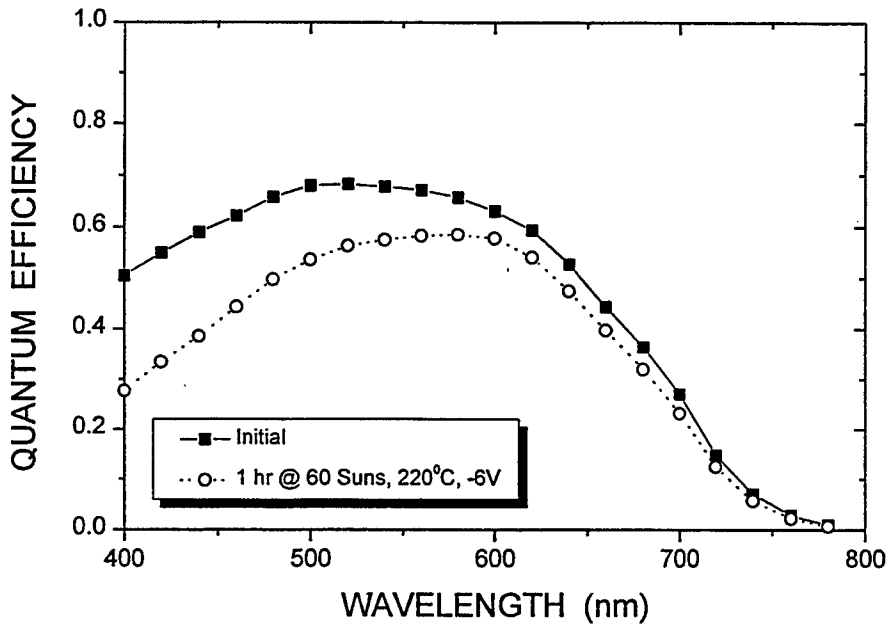

Fig. 4.28 The spectral response of an a-Si:H cell before and after exposure to 60 suns for 1 hour at 220^0C at a reverse bias of - 6 V.

In summary, these experiments show that degraded a-SiGe:H cells exhibit field-enhanced recovery similar to that observed for a-Si:H cells, but the recovery process is slower for a-SiGe:H cells both in the dark and under intense illumination. If proton motion is involved in the field-enhanced recovery, then the data suggest that the protons move more slowly in a-SiGe:H than in a-Si:H. ***This is contrary to what was expected since hydrogen appears to move more rapidly in a-SiGe:H than in a-Si:H*** [24]. However, the field-enhanced recovery effects may be associated with the local motion of protons, and the reconstruction of local bonds near the metastable centers may be inhibited in a-SiGe:H alloys.

4.2.2 Single Junction a-SiGe:H Solar Cells with Helium- and Argon-Diluted i-Layers

We have been investigating helium and argon dilution of the source gases as a way to increase the deposition rate and also to reduce the light-induced degradation of the back junction by controlling the microstructure of the a-SiGe:H layers. Preliminary results show that a-SiGe:H single junction cells can be fabricated using helium-diluted i-layers with comparable efficiencies (both under AM 1.5 and red light illumination) to devices with hydrogen-diluted i-layers.

In Table 4.8, we show the initial and light-soaked efficiencies of a-SiGe:H single-junction cells where the intrinsic layers were fabricated using the optimum conditions for hydrogen, helium and argon dilution. The current voltage characteristics of the a-SiGe:H cells were measured using a red filter ($\lambda > 540$nm).

Table 4.8 Initial Performance and Degradation of a-SiGe Cells Fabricated using Different Dilution Gases

Sample #	Diluent	d (nm)	V_{oc} (V)	FF	J_{sc} (mA/cm^2)	Eff. (%)	J_{sc} (QE) (mA/cm^2)	QE (800nm)	Degrad. (%) (60sun/0.5h)
C7149	H	206	0.66	0.60	9.8	3.9	17.0	0.231	27.5
C7205	He	162	0.66	0.66	8.5	3.7	16.6	0.151	25.0
MC7120	Ar	199	0.63	0.61	9.4	3.6	17.0	0.200	22.0

From the table we can see that the initial efficiency of the single-junction a-SiGe:H cells fabricated using helium dilution is comparable to that of hydrogen-diluted cells although the deposition rate was ~ 20% higher with helium dilution. The helium-diluted cells exhibit about 25% degradation under accelerated light soaking (60 suns for 30 minutes) as compared to about 27.5% for the hydrogen-diluted cells. Thus, the performance of hydrogen- and helium-diluted single-junction cells is comparable both for the annealed and light-soaked states. The cells made using argon dilution exhibit a somewhat lower degradation (~ 22%), but the initial performance was ~ 10% less than that of the hydrogen- and helium-diluted cells. The IV characterization data in Table 4.8 (and in Table 4.9 below) has been performed using simulated 1 sun illumination through a red filter ($\lambda > 560$nm).

4.2.3 Effect of Substrate Temperature on the Red Response of a-SiGe:H Cells

The main precursors for the growth of the a-SiGe:H alloys are believed to be the SiH_3 and GeH_3 radicals. Moreover, heavy species like GeH_2 which have a high sticking coefficient also take part during the growth of a-SiGe:H alloys. GeH_2 and GeH_3 precursors are relatively heavy and need a lot of energy and momentum to find energetically favorable sites on the growing surface. This energy for the growth of an improved microstructure could come from the energetic species in a strong hydrogen- or helium-diluted discharge or from the heated substrate.

We varied the substrate temperature from 200 to 275^{0}C during the growth of the intrinsic layers of single-junction a-SiGe:H cells and the results are displayed in Table 4.9. The efficiency measured with a red filter ($\lambda > 540$ nm) decreases as the substrate temperature increases from 200 to 275^{0}C due mainly to a decrease in V_{OC} and in the fill factor. The quantum efficiency at 800 nm increases as the substrate temperature increases due to a decrease in the band gap, but the quantum efficiency at 400 nm decreases probably due to outdiffusion of hydrogen from the p/i interface region.

Table 4.9 PV Parameters for a-SiGe:H Cells Made at Different Values of T_S

Run #	d (nm)	T_s (C)	V_{oc} (V)	FF	J_{sc} (mA/cm^2)	Eff. (%)	J_{sc} (QE) (mA/cm^2)	QE (400nm)	QE (800nm)
C7149-2	206	200	0.66	0.60	9.8	4.0	17.0	0.58	0.222
C7149-3	190	250	0.60	0.60	9.6	3.5	17.0	0.53	0.322
C7149-4	197	275	0.55	0.51	9.9	2.9	16.6	0.471	0.339

4.3 Task 3: Multijunction Devices and Modules

4.3.1 Development of a Fast Tunnel/Recombination Junction Process

In an a-Si:H/a-SiGe:H tandem device structure, the time it takes to deposit the front junction, the back junction and the tunnel/recombination junction is roughly the same. Since an increase in the deposition rate of the intrinsic layers has a detrimental effect on stability, we placed a priority on reducing the deposition time for the tunnel/recombination junction.

Our first efforts to speed up the deposition of the tunnel/recombination junction in our tandem devices resulted in a reduction in the total process time of about 8%. The open-circuit voltages and fill factors of the cells fabricated using this faster tunnel/recombination junction process (H-5-1) is comparable to our standard (H-5) recipe as shown in Fig. 4.29 and Fig. 4.30, respectively. Each data point in the figures represents an average of 6 - 12 cells. The average open-circuit voltage of the H-5-1 samples (1.54 V) was slightly larger than that of H-5 cells (1.53 V), but the average fill factor was slightly lower (0.647 to 0.653). Data from spectral response measurements are shown in Table 4.10 for cells made using the H-5 and H-5-1 recipes. The samples H7329-1 and H7329-2 were made under identical conditions except for the tunnel/recombination junction. The QE measurements indicate that both the red response and short circuit current of the a-SiGe:H back junction were improved by using the H-5-1 recipe.

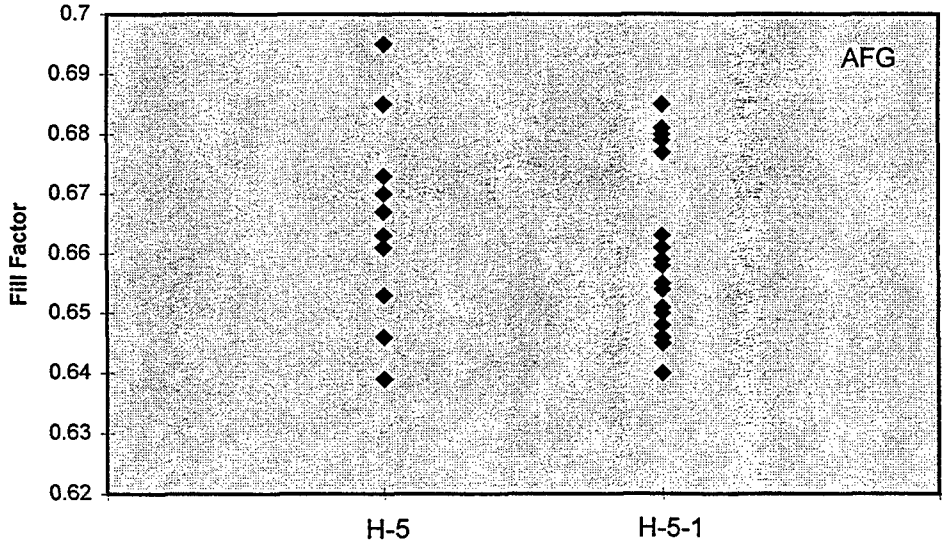

Fig. 4.29 A comparison of the FF values obtained using the standard (H-5) and the faster (H-5-1) tunnel/recombination junction recipes.

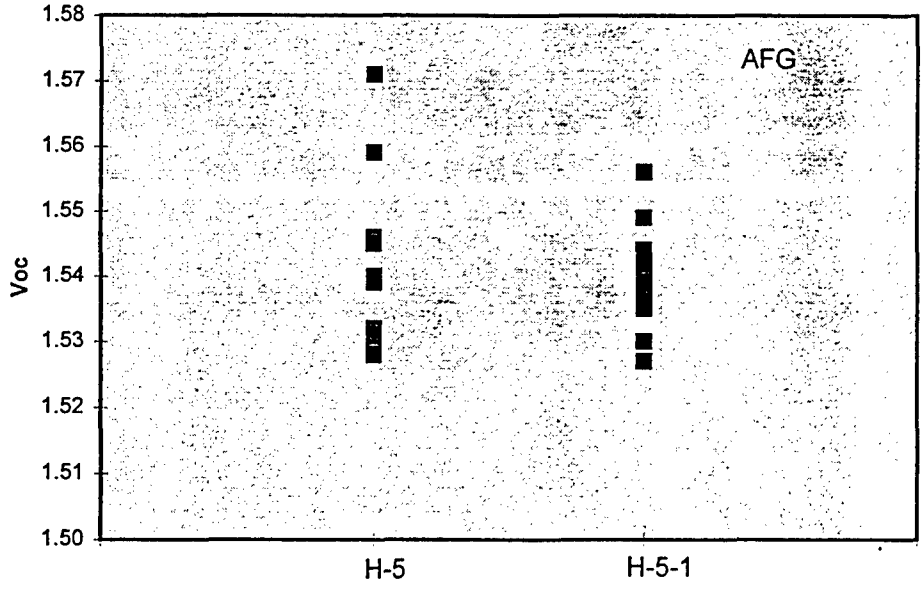

Fig. 4.30 A comparison of the V_{OC} values obtained using the standard (H-5) and the faster (H-5-1) tunnel/recombination junction recipes.

Table 4.10 Comparison of current density and quantum efficiency of cells fabricated using the standard (H-5) and faster (H-5-1) recipes

Cell	*Recipe*	*Jsc1 (QE) (mA/cm2)*	*Jsc2(QE) (mA/cm2)*	*QE (800nm)*
H7329-1MB	H-5	8.61	7.95	0.192
H7329-2MB	H-5-1	8.82	8.16	0.226

Modules (12" x 13") were fabricated using these two recipe on commercial tin oxide coated glass. The module performances were also similar with initial efficiencies ranging from 8.3 to 8.5 %.

The light-induced degradation of solar cells fabricated using the two recipes was also examined, and the normalized efficiencies as a function of time are shown in Fig. 4.31. As shown in the figure, the light-induced degradation of the cells fabricated using the two recipes was comparable.

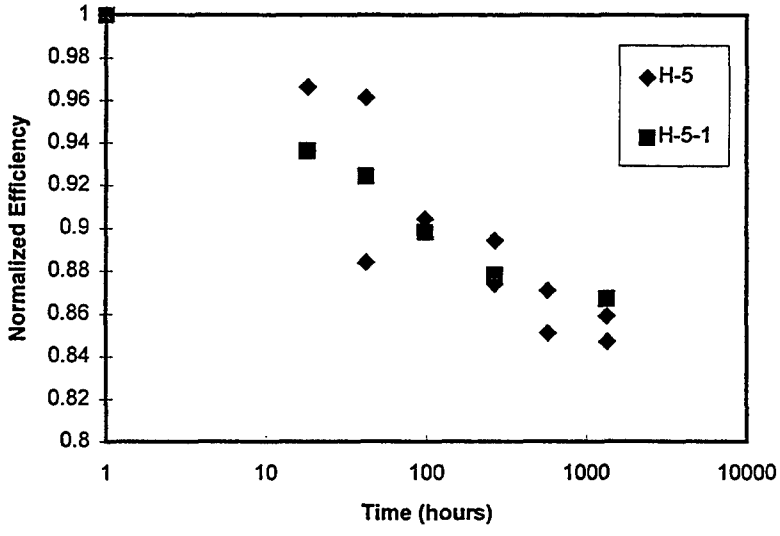

Fig. 4.31 Comparison of the degradation of the normalized efficiency of cells fabricated using the standard (H-5) and the faster (H-5-1) tunnel/recombination junction processes.

More recently, we have performed a number of additional experiments to try to further reduce the time for the formation of the tunnel/recombination junction. We have tried varying a number of deposition conditions (such as the discharge power, the hydrogen dilution, the flush times, etc.) during the formation of the tunnel/recombination junction and have developed two even faster processes. Table 4.11 shows the relative processing times for these new fast tunnel/recombination junction processes as compared to our standard process.

Table 4.11 The Relative Processing Time for Our Standard Tunnel/Recombination Junction Process and Three Faster Processes.

	Standard	*FST 1*	*H-5-1*	*FST 2*	*FST 3*
Relative Processing Time	1.0	0.729	0.483	0.389	0.389

The deposition of the microcrystalline (μc) n+ layer is one of the longest steps in our standard tunnel/recombination junction process. In order to speed up the deposition of the μc-n+ layer, we varied the deposition conditions so as to reduce ion-damage during growth of crystallites [25]. To determine the quality of these μc-n+ layers we used a simplified tunnel/recombination junction structure. This test junction yielded a somewhat lower Voc and FF but reflected the properties of the μc-n+ layer. Deposition conditions such as the degree of hydrogen dilution were varied while monitoring the photovoltaic characteristics.

Optimization of the deposition conditions for the μc-n+ layer has led to three faster processes, FST 1, FST 2, and FST 3 with successive faster times for deposition. As shown in Table

4.12, the performances of the cells prepared using these three faster processes are close to that observed using the standard process.

Table 4.12 The performance of cells prepared using the standard tunnel/recombination junction and three faster processes.

Process	*Initial Eff.(%)*	*FF*	*Voc*	*Rs*	*Jsc QE (mA/cm2)*	*Sample #*
Standard	8.41	0.67	1.55	15	8.1	7321-3c
	7.81	0.70	1.55	15	7.2	7269-2c
	8.13	0.69	1.55	15	7.6	7272-1c
FST 1	7.84	0.67	1.54	16	7.6	7335-5c
FST 2	7.8	0.65	1.55	21	7.8	7364-4c
FST 3	7.89	0.67	1.55	22	7.6	8029-3c

4.3.2 Development of a Fast Deposition Process with a Reduction in Feedstock Flows

The total process time for depositing the a-Si:H/a-SiGe:H structure has been reduced significantly by incorporating the H-5-1 fast recombination junction process described in the previous section with a 2-step process for the intrinsic layer in the first junction. In addition, both feedstock flows were reduced by 30% as compared to our standard H-5 process. As shown in Table 4.13, the "F7" process reduced the total process time by 12% while the "F0" process reduced the time by 21%. As also shown in the table, the performance of these "fast process" cells are similar to or better than those of the standard control cells.

Table 4.13 Cell Performance using Fast Process Recipes

Cell #	*Voc (V)*	*FF*	*Jsc (QE) (mA/cm2)*	*QE (800nm)*	*Eff. (%)*	*Process Time Reduction*
Control-1	1.542	0.697	8.16	0.208	8.76	0%
Control-2	1.555	0.671	8.28	0.187	8.64	0%
F7-1	1.558	0.684	8.21	0.236	8.86	12%
F7-2	1.532	0.701	8.16	0.231	8.76	12%
F0-1	1.522	0.722	8.48	0.267	9.32	21%
F0-2	1.545	0.708	8.51	0.282	9.31	21%
F0-3	1.551	0.715	8.45	0.263	9.37	21%
F0-4	1.554	0.713	8.60	0.288	9.53	21%

Data for the light-induced degradation of control cells and the cells made with the F7 process are shown in Fig. 4.32, and the degradation is similar.

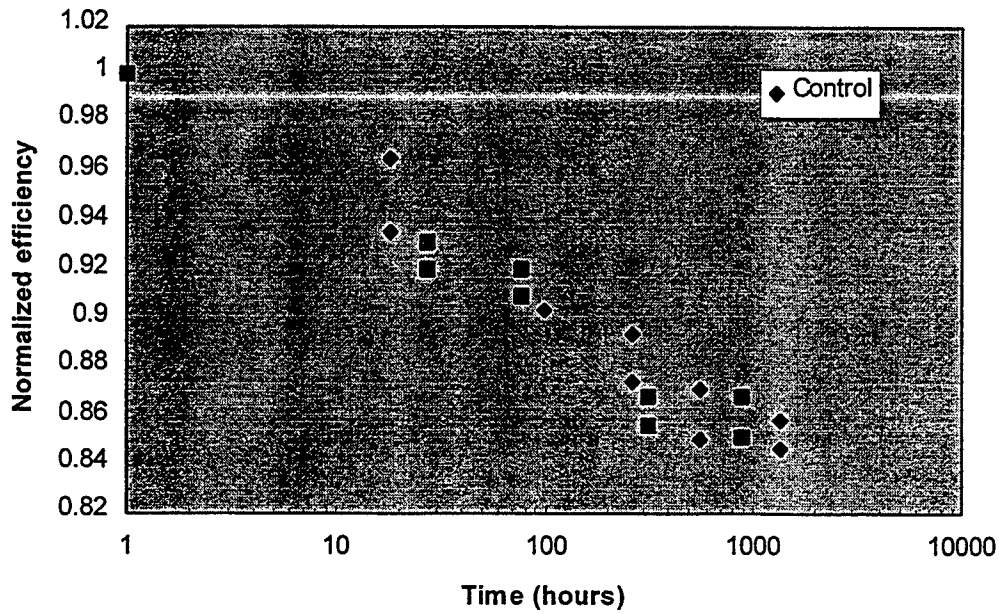

Fig. 4.32 The normalized efficiency of cells prepared using the control process and the F7 process as function of light soaking time (simulated 1 sun illumination).

4.3.3 Comparison of Tandem Cell Performance and Degradation with Different Glass Cleaning Procedures

Commercial tin oxide coated glass is usually shipped with a protective coating such as adipic acid. This coating can be difficult to remove, and the residue can adversely affect device performance. Thus, a set of experiments was designed to compare the effects of different cleaning processes. Four different types of samples were prepared using commercial tin oxide coated glass. The first group of samples consisted by 3" by 3" plates that were cleaned in an ultrasonic detergent bath. The second group started with a 12" by 13" plate that was first cleaned in an ultrasonic bath, and was then cut into 3" by 3" plates. The third group was cleaned using our normal glass washing process. The fourth group was similar to third, but the plates were subjected to a high temperature treatment (500 ^{0}C) before being cleaned in the commercial glass washer. The results, shown in Table 4.14, indicated that the best cell performance was obtained with the ultrasonic cleaning method.

Table 4.14 Tandem Solar Cell Performance For Different Clean Processes

Samples	*Fill Factor*	*Voc (V)*	*Rs*	*Cleaning Method*
H8069-2LTM	0.720	1.554	16.18	1, Ultrasonic Bath
H8069-2RTM	0.712	1.540	17.18	1, Ultrasonic Bath
H8069-2RB	0.721	1.566	18.54	2, Ultrasonic Bath
H8069-2RT	0.727	1.568	17.18	2, Ultrasonic Bath
H8068-2LB	0.637	1.514	34.34	3, Normal
H8068-2LT	0.631	1.515	27.89	3, Normal
H8069-2LB	0.671	1.523	24.20	4, High Temp. Treatment
H8069-2LT	0.684	1.541	22.74	4, High Temp. Treatment

Since the boiling point of adipic acid is 265 °C, the high temperature treatment (500 °C) should remove most of the adipic acid. However, as shown in Table 4.14, the performance of the cells whose substrates were treated at high temperatures was inferior to cells where the substrates were cleaned in an ultrasonic bath. This result indicates that some surface residue still exists after the high temperature treatment.

Since alcohol dissolves adipic acid, we tried to clean the tin oxide surfaces by dipping the coated glass into an alcohol solution. However, this process left a white residue on the surface, and the cell performance was not improved.

We also performed experiments to determine whether the substrate cleaning method affected the light-induced degradation, and the results are shown in Fig. 4.33. Each data point in the figure represents an average of 7 to 12 single-junction devices where the substrates were either cleaned using a commercial glass washer or using an ultrasonic detergent bath. As shown in the figure, the light-induced degradation was somewhat less when the substrates were cleaned using an ultrasonic bath. Since the initial performance was about 14% higher for devices made on ultrasonically cleaned substrates, the stabilized performance is about 22% higher than those made on substrates cleaned with a commercial washer. Thus, the performance of a-Si:H solar cells fabricated on commercial tin oxide coated glass can be adversely affected unless the proper cleaning procedures are used to remove the protective coatings.

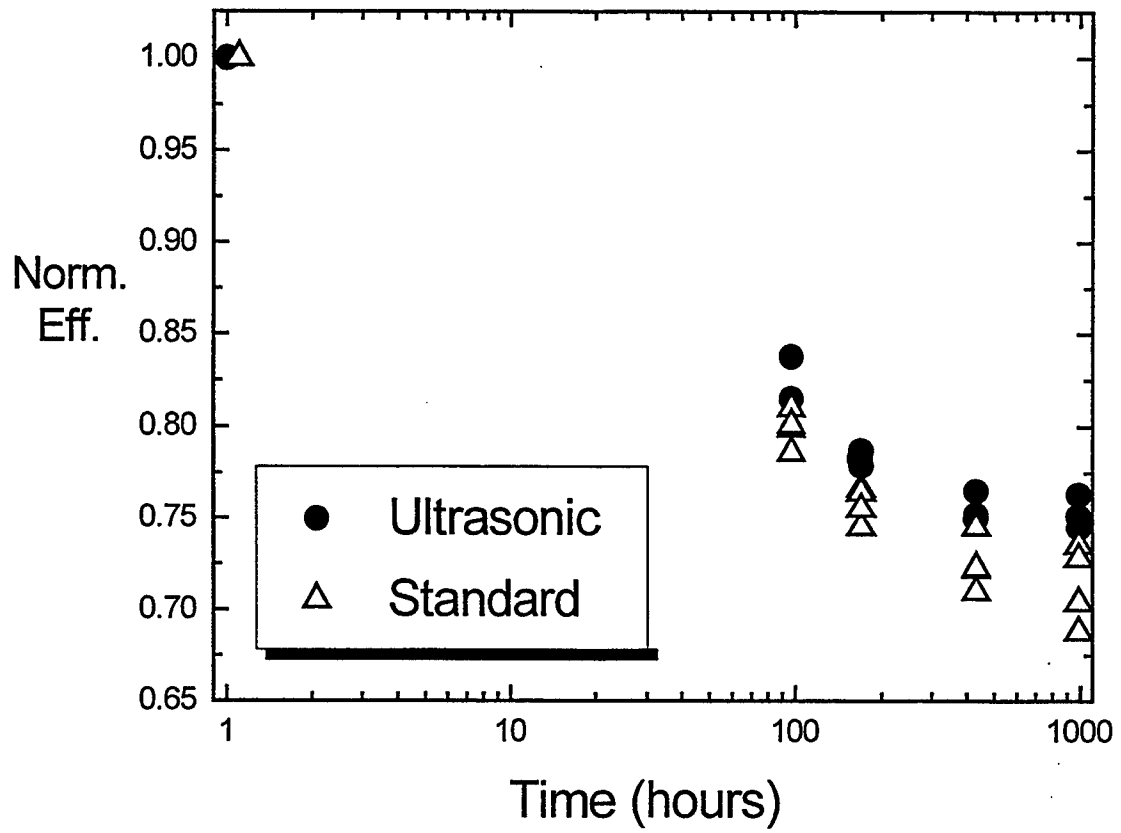

Fig. 4.33 The normalized conversion efficiency as a function of light-soaking time for p-i-n cells where the substrates were cleaned with either an ultrasonic bath or a standard commercial glass washer.

4.3.4 Development of Faster Processing of a-Si:H/a-SiGe:H Tandem Devices Using Helium Dilution

As mentioned in previous sections, both single-junction a-Si:H and a-SiGe:H cells have been developed using helium dilution, and these cells exhibit initial and stabilized efficiencies similar to that of standard hydrogen-diluted cells. Moreover, the deposition rate is found to increase by as much as 80% for a-Si:H and by 20% for a-SiGe:H alloys when helium is used as the diluent rather than hydrogen. In order to reduce the total process time of our tandem devices, we fabricated a-Si:H/a-SiGe:H devices on tin oxide coated glass substrates using helium diluted intrinsic layers in both junctions. We used tin oxide coated glass purchased from AFG and Asahi Glass in this study. All tandem cells were fabricated with the structure: glass/SnO_2/p-i_1-n/p-i_2-n/ZnO/Al where the i_1 layer was intrinsic a-Si:H and the i_2 layer was intrinsic a-SiGe:H. The thicknesses of the intrinsic layers were adjusted in order to match the currents from the front and back junctions. The initial performance of these tandem devices is shown in Table 4.15.

Table 4.15 Photovoltaic Properties of Tandem Cells Made with Helium Dilution

Run #/ SnO_2	*V_{oc} (V)*	*FF*	*J_{sc1}/J_{sc2} (mA/cm^2)*	*Eff. (%)*	*QE (700nm)*	*Degrad. in Eff. (%)*
C7223-1 *Asahi*	1.52	0.71	8.38/8.64	9.18	54.5	20.5
C7223-2 *Asahi*	1.52	0.70	8.47/7.67	8.59	46.6	17.2
C7225-1 *AFG*	1.516	0.68	8.27/7.27	8.01	48.5	12.3
C7226-1 *AFG*	1.50	0.715	8.27/8.2	8.84	56.0	18.0

The last column in Table 4.15 lists the amount of degradation induced by exposure to 60 suns illumination for 30 minutes at 60^0C. The degradation is in the range of 12 to 21% which is comparable to that observed in standard hydrogen-diluted tandem devices. The kinetics of the light-induced degradation for several samples under AM 1.5 illumination is shown in Figs. 4.34 and 4.35. While there is no clear evidence of saturation in the light-soaking data in Figs. 4.34 and 4.35, the degradation after 600 hours of exposure is similar to that observed with cells made using hydrogen dilution. Thus, the total process time for the fabrication of tandem devices has been reduced by about 17% by using helium dilution while the stabilized photovoltaic performance is comparable to standard hydrogen-diluted devices.

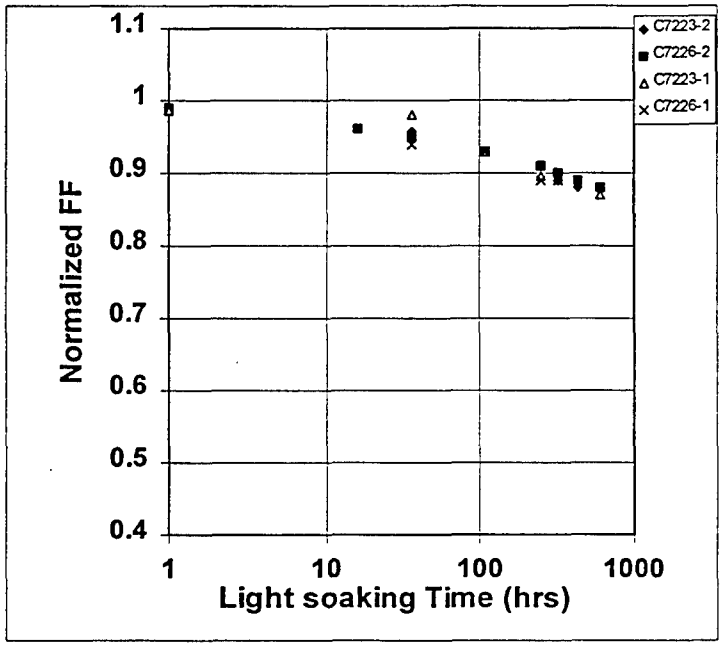

Fig. 4.34 The change in normalized fill factor with light soaking time for several tandem cells.

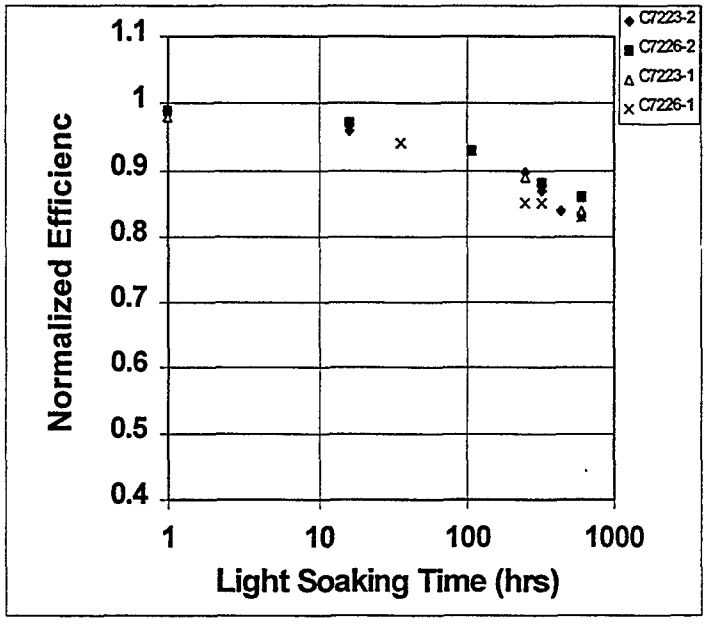

Fig. 4.35. The change in normalized efficiency with light soaking time for several tandem cells.

Varying the deposition conditions associated with the hydrogen dilution technique can also increase the deposition rate. However, it is generally observed that the light-induced degradation of a-Si:H and a-SiGe:H cells grown with hydrogen dilution decreases with increasing deposition rate. We have observed that the light-induced degradation is comparable for both single-junction and tandem cells made with helium dilution at deposition rates about twice those of cells made with hydrogen dilution. These good results with helium dilution may be related to a compact network structure and a predominately mono-hydride bonding configuration. This structural modification of the helium-diluted films probably results from the large amount of energy that is transferred to the growing surface by the de-excitation of metastable helium atoms and ions.

4.3.5 LPCVD ZnO Contacts

The following figures summarize some recent experiments where the ZnO was grown using LPCVD with a proprietary organometallic feedstock in a nitrogen carrier gas. Figs. 4.36, 4.37 and 4.38 show the effect of substrate temperature on the fill factor, series resistance and open-circuit voltage, respectively, for tandem cells coated with ZnO in an LPCVD bell jar system. All three photovoltaic parameters start to degrade when the set point temperature reaches 215^{0}C (the actual substrate temperature is about 207^{0}C). The rapid increase in the series resistance may be due to the formation of a resistive silicon oxide layer at the interface. The deposition rate increased from ~ 1.2 nm/s at an actual substrate temperature of ~ 157^{0}C to ~ 7.8 nm/s at ~ 207^{0}C.

We have also found that the pressure in the LPCVD system can affect the quality of the devices. For pressures greater than about 5 Torr, the performance of tandem cells decreased due to a decrease in the fill factor (caused by an increase in the series resistance). In another

experiment, we examined the effect of exposing the a-Si:H to air for varying times before depositing the ZnO. We found that no significant loss in performance occurred if the a-Si:H tandem structure was exposed to air for 1 day before depositing the ZnO, but after one week of exposure to air, the performance decreased due to an increase in series resistance.

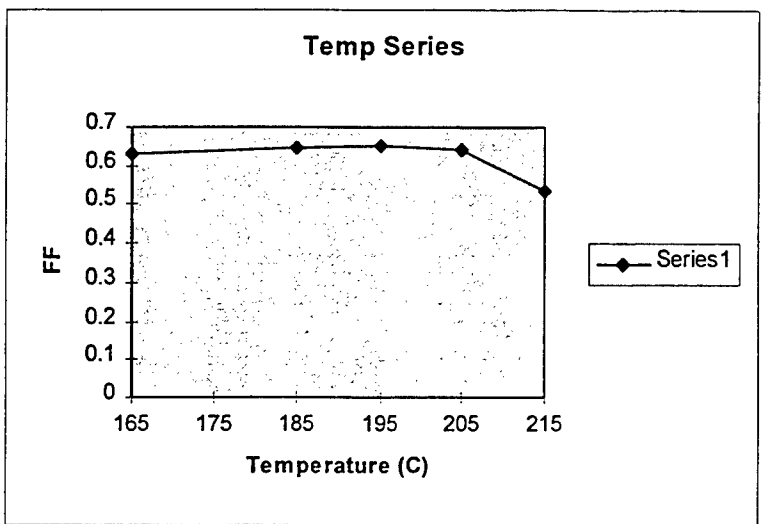

Fig. 4.36 The fill factor of tandem cells vs. set point temperature.

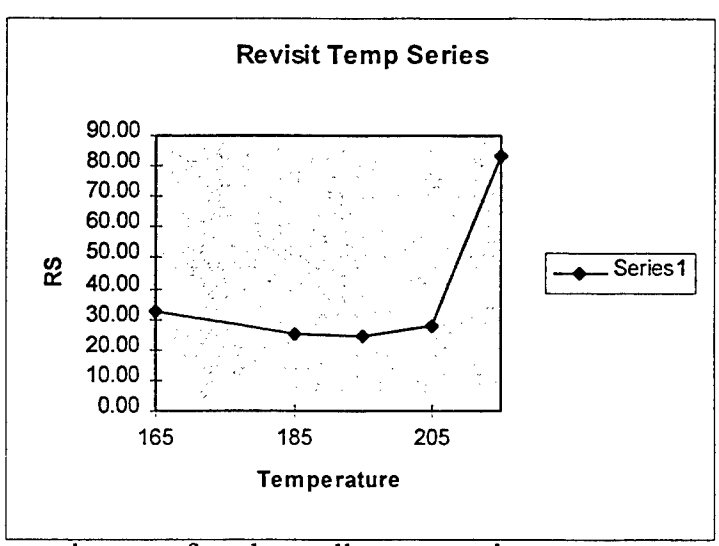

Fig. 4.37 The series resistance of tandem cells vs. set point temperature.

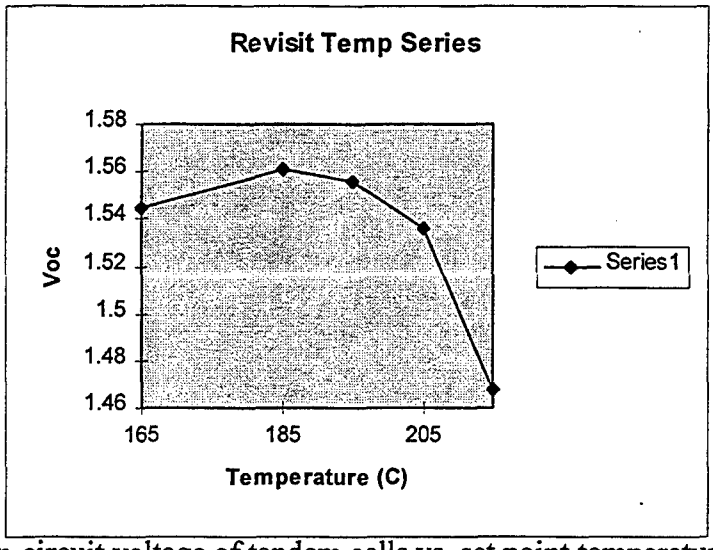

Fig. 4.38 The open-circuit voltage of tandem cells vs. set point temperature.

4.3.6 Performance of Large-Area Tandem Modules

The process developed in R&D for the fabrication of a-Si:H/a-SiGe:H devices was scaled up to 4 ft^2 using glass coated in house with textured tin oxide. More than 3000 modules (36" x 16") were fabricated over a period of about two years. The data shown in Fig. 4.39 represents a run of 40 modules made sequentially over a period of a few days in a large-area load-lock deposition system. As shown in the figure, the average initial conversion efficiency was 9.5% with the best module exhibiting an efficiency of 10.04%. Based on light soaking data for similar modules, the average stabilized conversion efficiency is projected to be about 8.1%.

These results show that the tandem process can be scaled up to large areas in a pilot production mode with high yields. More recently the tandem process has been transferred to a plant in Virginia that is capable of producing 10 MW/year of 8.6 ft^2 tandem modules.

5. Summary

The Solarex R&D program has been focused for the last few years on developing a high performance amorphous silicon tandem process and on scaling it up to large areas. Significant progress has been made in several areas: (1) improved understanding of the light-induced degradation of amorphous silicon alloys, (2) the processing time for tandem device structures has been reduced by 21%, (3) the feedstock gas utilization has been increased by 30%, (4) stabilized conversion efficiencies of more than 8% have been demonstrated in 4 ft^2 tandem modules made in a pilot production mode, and (4) the tandem module process has been transferred to a Solarex manufacturing plant in Virginia that is capable of producing 10 MW of 8.6 ft^2 tandem modules per year.

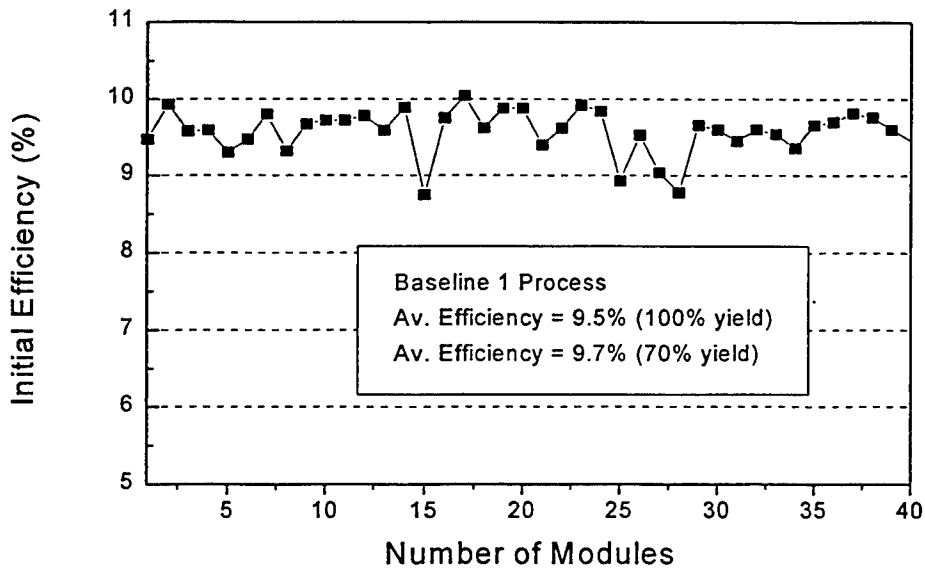

Fig. 4.39 Run chart for the initial conversion efficiency of baseline 1 process modules (4 ft^2) made in a pilot production run.

6. Acknowledgments

The authors would like to acknowledge the contributions of M. Bennett, K. Jansen, Y.-L. Li, N. Maley, J. Newton, K. Rajan, F. Willlling and L. Yang in the earlier phases of this work.

7. References

1. D. L. Staebler and C. R. Wronski, Appl. Phys. Lett. **31**, 292 (1977).

2. D. L. Staebler, R. S. Crandall and R. Williams, Conf. Record of the 15th IEEE Photovoltaic Specialists Conf. (IEEE, NY 1981) p. 249.

3. A. Delahoy and T. Tonon, Proc. of the International Conference on Stability of Amorphous Silicon Alloy Materials and Devices, Colorado, 1987. p. 263.

4. H. Dersch, J. Stuke and J. Beichler, Appl. Phys. Lett. **38**, 456 (1980).

5. M. Gunes, C. R . Wronski and T. J. McMahon, J. Appl. Phys. **76** [4] 2260 (1994).

6. D. E. Carlson, R. R. Arya, M. Bennett, L.-F. Chen, K. Jansen, Y.-M. Li, J. Newton, K. Rajan, R. Romero, D. Talenti, E. Twesme, F. Willing and L. Yang, Conf. Record of the 25th IEEE Photovoltaic Specialists Conf. (IEEE, NY 1996) p. 1023.

7. P. Stradins and H. Fritzsche, J. Non-Cryst. Solids 198-200, 432 (1996).

8. D. E. Carlson and K. Rajan, Appl. Phys. Lett. **68** [1] 28 (1996).

9. D. E. Carlson and K. Rajan, Appl. Phys. Lett. **69** [10] 1447 (1996).

10. D. E. Carlson, Appl. Phys. A **41**, 305 (1986).

11. D. E. Carlson and K. Rajan, Appl. Phys. Lett. **70** [16] 2166 (1997).

12. B. W. Faughnan and R. S. Crandall, Appl. Phys. Lett. **44**, 537 (1984).

13. D. E. Carlson and C. Magee, Appl. Phys. Lett. **33**, 81 (1978).

14. P. V. Santos, N. M. Johnson and R. A. Street, Phys. Rev. Lett. **67**, 2686 (1991).

15. H. Dersch, J. Stuke and J. Beichler, Appl. Phys. Lett. **38**, 456 (1981).

16. A. G. Gaydon, "Dissociation Energies and Spectra of Diatomic Molecules", John Wiley & Sons, NY 1947.

17. A. K. Johscher, in "Electronic and Structural Properties of Amorphous Semiconductors" (P. G. LeComber and J. Mort, eds.), pp. 329-361. Academic Press, NY 1973.

18. G. A. Swartz, Appl. Phys. Lett. **44**, 697 (1984).

19. K. Tanaka and A. Matsuda, Thin Solid Films **163**, 123 (1988).

20. S. Hazra, A.R. Middya, and S. Ray, J. Appl. Phys. **78**, 581 (1995).

21. H. Shirai, T. Ariyoshi, J. Hanna, and I. Shimizu, J. Non-Cryst. Solids, **137** & **138**, 693 (1991).

22. D. E. Carlson and K. Rajan, J. Appl. Phys. **83** [3] 1726 (1998).

23. D. E. Carlson and K. Rajan, *14th European Photovoltaic Solar Energy Conf., Barcelona, Spain*, 30 June 1997 - 4 July 1997, pp. 652-655.

24. M. Heintze, K. Eberhardt, O. Tress and G. H. Bauer, J. Non-Cryst. Solids **137 & 138**, 49-52 (1991).

25. G. Ganguly et. al. , J. Non-Cryst. Solids, *Proc. ICAMS 17, Budapest, Hungary* (1997)

REPORT DOCUMENTATION PAGE

Form Approved
OMB NO. 0704-0188

1. AGENCY USE ONLY (Leave blank)	2. REPORT DATE	3. REPORT TYPE AND DATES COVERED
	June 1998	Final Technical Report; 13 September 1994 – 28 February 1998

4. TITLE AND SUBTITLE
Amorphous Silicon Research, Final Technical Report, 13 September 1994–28 February 1998

5. FUNDING NUMBERS
C: ZAN-4-13318-01
TA: PV804404

6. AUTHOR(S)
R. Arya, D. Carlson, L. Chen, G. Ganguly, M. He, G. Lin, R. Middya, S. Skibo, and G. Wood

7. PERFORMING ORGANIZATION NAME(S) AND ADDRESS(ES)

Solarex, a business Unit of Amoco/Enron Solar
826 Newtown-Yardley Road
Newtown, PA 18940

8. PERFORMING ORGANIZATION REPORT NUMBER

9. SPONSORING/MONITORING AGENCY NAME(S) AND ADDRESS(ES)

National Renewable Energy Laboratory
1617 Cole Blvd.
Golden, CO 80401-3393

10. SPONSORING/MONITORING AGENCY REPORT NUMBER

SR-520-24854

11. SUPPLEMENTARY NOTES

NREL Technical Monitor: K. Zweibel

12a. DISTRIBUTION/AVAILABILITY STATEMENT
National Technical Information Service
U.S. Department of Commerce
5285 Port Royal Road
Springfield, VA 22161

12b. DISTRIBUTION CODE

13. ABSTRACT *(Maximum 200 words)*

The Solarex research and development program has focused for the last few years on developing a high-performance amorphous silicon tandem process and on scaling it up to large areas. Significant progress has been made in several areas: (1) improved understanding of the light-induced degradation of amorphous silicon alloys, (2) the processing time for tandem device structures has been reduced by 21%, (3) the feedstock gas utilization has been increased by 30%, (4) stabilized conversion efficiencies of more than 8% have been demonstrated in 4-ft^2 tandem modules made in a pilot production mode, and (4) the tandem module process has been transferred to a Solarex manufacturing plant in Virginia that is capable of producing 10 MW of 8.6-ft^2 tandem modules per year.

14. SUBJECT TERMS

photovoltaics ; amorphous silicon solar cells ; mid-gap amorphous silicon ; low-bandgap amorphous silicon alloys ; multijunction devices and modules

15. NUMBER OF PAGES
55

16. PRICE CODE

17. SECURITY CLASSIFICATION OF REPORT	18. SECURITY CLASSIFICATION OF THIS PAGE	19. SECURITY CLASSIFICATION OF ABSTRACT	20. LIMITATION OF ABSTRACT
Unclassified	Unclassified	Unclassified	UL

Report Number (14) NREL/SR--520-24854

Publ. Date (11) 199806

Sponsor Code (18) DOE/EE, XF

UC Category (19) UC-1250, DOE/ER

ph